

University of Tartu
Faculty of Science and Technology
Institute of Technology

Erik Ilbis

**System Architecture and Component Evaluation for
ESTCube-2 Electrical Power System**

Master's Thesis in Computer Engineering (30 ECTS)

Supervisors:

Mihkel Pajusalu, PhD

Artur Abels, BSc

Tartu 2016

ABSTRACT / RESÜMEE

System Architecture and Component Evaluation for ESTCube-2 Electrical Power System

This thesis is focused on the architecture of the electrical power system (EPS) and implementations of the various subsystems within the EPS for ESTCube-2 nanosatellite. The main goals are to establish a high level system architecture compatible with the rest of the satellite and investigate solutions for the battery management and protection (BMPS) and the voltage conversion and power distribution systems (VCPDS).

In this work, an overview is given of the ESTCube-2 mission and the satellite's architecture. Based on the satellite architecture, requirements are set for the EPS subsystems to be investigated. For the BMPS, two hot-swap controller based solutions are investigated, prototyped and tested. For the VCPDS, two load switch designs are evaluated, six different voltage converters are characterized and solutions for the power distribution system are proposed. Based on the testing results, recommendations are made for the final implementation.

Keywords: ESTCube-2, CubeSat, electrical power system, battery management, hot-swap controller, DC/DC converter, component evaluation

Süsteemi arhitektuur ning komponentide valimine ESTCube-2 toitealamsüsteemi jaoks

Käesolev lõputöö keskendub ESTCube-2 nanosatelliidi toitealamsüsteemi arhitektuurile ning süsteemi jaoks tarvilike komponentide valimisele. Töö peamised eesmärgid on luua kavand toitealamsüsteemi ülesehituse jaoks, mis oleks ühilduv ülejäänud satelliidiga, ning arendada välja akuhaldussüsteem ning pingemuundamis- ja energijaotussüsteem.

Töös antakse ülevaade ESTCube-2 missioonist ning satelliidi arhitektuurist. Viimasele tuginedes koostatakse nõuded arendatavate süsteemide jaoks. Akuhaldussüsteemi jaoks luuakse kaks prototüüpi, mis põhinevad käigultvahetuse kontrollritel. Pingemuundamis- ja energijaotussüsteemi jaoks uuritakse kahte erinevat võimsuslülituse lahendust ning katsetatakse kuut erinevat pingemuundurit. Samuti pakutakse välja lahendused energia jaotamiseks teistele alamsüsteemidele. Testimistulemuste alusel tehakse soovitud lõpplahenduse jaoks.

Võtmesõnad: ESTCube-2, CubeSat, toitealamsüsteem, akuhaldus, impulsspingeregulaator, komponendi valik

CERCS: T120, T170, T161, T320

TABLE OF CONTENTS

- Abstract 2
- List of figures 5
- List of tables 7
- Acronyms and abbreviations 8
- 1. Introduction 10
- 2. Overview 12
 - 2.1. Overview of the ESTCube-2 mission 12
 - 2.2. Overview of other electrical power systems 13
 - 2.3. Lessons learned from ESTCube-1 EPS 13
 - 2.4. Space environment hazards 14
 - 2.4.1. Component de-rating 15
- 3. System architecture 17
 - 3.1. Satellite architecture 17
 - 3.2. EPS block diagram 18
 - 3.3. Power budget analysis 20
- 4. Methodology and measurements 23
 - 4.1. Voltage converter performance evaluation 23
 - 4.2. Base testing platform 23
 - 4.2.1. Converter efficiency 25
 - 4.2.2. Output voltage ripple 25
 - 4.2.3. Transient response 26
 - 4.2.4. Near-field electromagnetic emissions 26
 - 4.2.5. Testing methodology and data analysis 27
- 5. Battery management and protection 28
 - 5.1. Requirements 28
 - 5.2. General system design 28

5.3.	Battery balancing	28
5.4.	Under- and overvoltage protection	30
5.5.	Load switch design	30
5.5.1.	LTC4226 based design	31
5.5.2.	LTC4228 based design	34
5.6.	Testing results	35
6.	Voltage conversion and power distribution	39
6.1.	Requirements	39
6.1.1.	Voltage conversion system design	39
6.2.	Conversion input stage design	40
6.3.	Method for voltage conversion	42
6.4.	Converter evaluation and selection	44
6.4.1.	Voltage conversion efficiency	46
6.4.2.	Voltage stability	48
6.4.3.	Output voltage ripple	49
6.4.4.	Transient response	51
6.4.5.	Near-field electromagnetic emissions	52
6.4.6.	Converter testing conclusion	52
6.5.	Converter output OR connection and load sharing	53
6.6.	Power distribution circuitry	54
7.	Summary	56
8.	Kokkuvõte	57
	Acknowledgements	58
	Appendix – Additional measurement results	64

LIST OF FIGURES

Figure 1. Satellite’s system architecture overview. Payloads are external to the system 17

Figure 2. Computer render of a proposed solution for the bus (Credit: Iaroslav Iakubivskiy)18

Figure 3. Electrical Power System block diagram. The bold arrows represent current flow and dashed lines illustrate control and measurement interfaces. 19

Figure 4. Block diagram of the measurement platform 23

Figure 5. Computer render of the regulator testing platform with certain devices and measurement locations highlighted. The highlighted dark red traces show the path of higher current throughout the platform. 24

Figure 6. Ripple measurement setup 26

Figure 7. LTC4226 based battery switch. Note: the diagram only illustrates the most critical connections needed for understanding the operation of the system. The physical implementation is more complex. 32

Figure 8. LTC4228 based battery switch. Note: the diagram only illustrates the most critical connections needed for understanding the operation of the system. The physical implementation is more complex. 34

Figure 9. Charge mode losses of power switches. The thick lines show the losses between voltages of 6.6 and 8.4 V 36

Figure 10. Discharge mode losses of power switches. The thick lines show the losses between voltages of 6.6 and 8.4 V 37

Figure 11. Voltage conversion system diagram 40

Figure 12. Voltage conversion input stage proposed solutions..... 40

Figure 13. DC/DC step-down converter basic construction. V_{IN} denotes the input voltage source and C_{OUT} denotes the output capacitor 42

Figure 14. DC/DC converter efficiency at 8.4 V input and 3.3 V output voltage in logarithmic scale emphasising light-load efficiency 47

Figure 15. Change in efficiency when input voltage is decreased from 8.4 V to 7.4 V. Larger values indicate larger increase in efficiency 48

Figure 16. DC/DC voltage stability at 8.4 V input and 3.3 V output voltage..... 49

Figure 17. Voltage conversion output stage..... 53

Figure 18. Calculated losses comparison between Schottky and ideal diode based circuits (Based on measurement data) 54

Figure 19. Voltage Conversion efficiency for LT8614 at three input voltages 64

Figure 20. Voltage Conversion efficiency for LTC3601 at three input voltages.....	64
Figure 21. Voltage Conversion efficiency for LTC3603 at three input voltages.....	65
Figure 22. Voltage Conversion efficiency for LTC3624 at three input voltages.....	65
Figure 23. Voltage Conversion efficiency for TPS51117 at three input voltages	66
Figure 24. Voltage Conversion efficiency for TPS62110 at three input voltages	66
Figure 25. LT8614 peak-to-peak ripple measurements	67
Figure 26. LTC3601 peak-to-peak ripple measurements.....	67
Figure 27. LTC3603 peak-to-peak ripple measurements.....	68
Figure 28. LTC3624 peak-to-peak ripple measurements.....	68
Figure 29. TPS51117 peak-to-peak ripple measurements	69
Figure 30. TPS62110 peak-to-peak ripple measurements	69
Figure 31. LT8614 RMS ripple measurements	70
Figure 32. LTC3601 RMS ripple measurements	70
Figure 33. LTC3603 RMS ripple measurements	71
Figure 34. LTC3624 RMS ripple measurements	71
Figure 35. TPS51117 RMS ripple measurements.....	72
Figure 36. TPS62110 RMS ripple measurements.....	72
Figure 37. LT8614 near-field EMI results (yellow 0.1 A, green 0.5 A, orange 1.5 A)	73
Figure 38. LTC3601 near-field EMI results (yellow 0.1 A, green 0.5 A, orange 1.5 A).....	73
Figure 39. LTC3603 near-field EMI results (yellow 0.1 A, green 0.5 A, orange 1.5 A).....	74
Figure 40. LTC3624 near-field EMI results (yellow 0.1 A, green 0.5 A, orange 1.5 A).....	74
Figure 41. TPS51117 near-field EMI results (yellow 0.1 A, green 0.5 A, orange 1.5 A)	75
Figure 42. TPS62110 near-field EMI results (yellow 0.1 A, green 0.5 A, orange 1.5 A)	75

LIST OF TABLES

Table 1. Recommended de-rating of parameters based on ECSS-Q-ST-30-11C revision 1 ... 16

Table 2. The preliminary power budget of ESTCube-2 bus 20

Table 3. Satellite bus operating mode for least power consumption (low power idle)..... 21

Table 4. Satellite bus operating mode for highest power consumption (active mission mode)
..... 21

Table 5. Comparison between the two proposed load switch designs 41

Table 6. Overview of the pros and cons of different DC/DC feedback systems 43

Table 7. Converter candidate overview..... 44

Table 8. Worst case ripple performance of the tested converter modules 50

Table 9. Transient response measurement results 51

Table 10. Battery management system charge voltage drop measurement results..... 76

Table 11. Battery management system discharge voltage drop measurement results 77

ACRONYMS AND ABBREVIATIONS

ADC – analog-to-digital converter

ADCS – attitude determination and control system

CMOS – complementary metal-oxide semiconductor

COM – communication subsystem

CSA – current sense amplifier

CSV – comma separated values

DAC – digital-to-analog converter

DC – direct current

DUT – device under test

EMI – electromagnetic interference

EPS – electrical power system

FET – field-effect transistor

FPGA – field programmable gate array

IO – input-output

LDO – linear dropout

LEO – low-Earth orbit

MCU – microcontroller unit

MLCC – multilayer ceramic capacitor

MOSFET – metal-oxide-semiconductor field-effect transistor

MPB – main power buss

MPPT – maximum power point tracking

MSOP – mini small outline package

NASA – National Aeronautics and Space Administration

OBC – on-board computer

OC – overcurrent

OV – over-voltage

PCB – printed circuit board

RMS – root mean square

PWM – pulse-width modulation

QFN – quad flat no leads

SEB – single event burnout

SEL – single event latch-up

SEU – single event upset

SMA – subminiature version A

ST – star tracker

UV – under-voltage

1. INTRODUCTION

Space is becoming more accessible by the year and is not no longer limited to large governmental agencies or corporations, but is also reachable for smaller research groups, start-ups and even individuals. Much of this is due to the emergence of the nanosatellites called CubeSats [1] in the early 2000s. The design guidelines enabling this revolution were developed in 1999 jointly by California Polytechnic State University and Stanford University. The first CubeSats were launched in 2003 and more than 400 have been launched since [2].

Most satellites need electrical energy in order to perform their mission. The energy has to be obtained, stored if needed and distributed to the consumers throughout the satellite. The aforementioned functions are usually fulfilled by the electrical power system (EPS). As this system is critical to the operation of the satellite, it must be capable of autonomous operation, including recovery from faults without suffering permanent damage. Requirements on the robustness and reliability are further increased by the fact that it is almost impossible to service or repair a spacecraft after it has been deployed into orbit. [3]

The conquest of space sparked the ESTCube programme, which was initiated at the University of Tartu in 2008 with an aim to provide students with hands-on experience in developing satellite hardware and software, and increase space technology research and development capabilities in Estonia. The first satellite, ESTCube-1 [4] was launched in 2013 into low-Earth orbit (LEO) where it successfully operated for two years until the official conclusion of its mission in the spring of 2015. The satellite eventually stopped operating due to severe degradation of its solar panels. The aim was to test the electric solar wind (E-Sail) technology [5]. Unfortunately, due to a malfunction in the tether deployment system, the experiment was not successfully completed [6].

This thesis focuses on the development of the EPS architecture, the battery management system, and the voltage conversion and power distribution system for the next satellite being developed within the ESTCube programme – ESTCube-2. The main objectives of this thesis are:

- List the requirements for the system blocks under study
- Develop a battery management system
- Develop a voltage conversion and power distribution system
- Test and verify the functionality and performance of the two aforementioned systems

This work contains the following sections:

- Chapter 2 gives an overview of the ESTCube-2 mission and the space environment
- Chapter 3 describes the proposed system's architecture of the satellite and the EPS
- Chapter 4 covers the different measurements taken and methods used to take them
- Chapter 5 focuses on the battery management and protection system's design and testing
- Chapter 6 investigates the voltage conversion and power distribution system
- Chapter 7 summarises the work covered in this thesis and discusses future development plans

This thesis covers the work done over the past two years.

2. OVERVIEW

2.1. OVERVIEW OF THE ESTCUBE-2 MISSION

ESTCube-2 nanosatellite will be three standard CubeSat units in size, measuring 10 x 10 x 34 cm and weighing a maximum of 4 kg. The spacecraft will be used for technology demonstration purposes. The current estimate foresees that the satellite would be completed by 2018 and launched to LEO soon afterwards. The satellite will use an in-house developed and built tightly integrated bus solution that includes all the essential functionalities of the satellite: an electrical power system (EPS), a communication system (COM), an attitude determination and control system (ADCS), a star tracker (ST) and an on-board computer (OBC). The aim is to make the bus as compact as possible in order to leave more room for the payloads. At the time of writing this thesis, the payloads for the satellite are not yet fixed. Multiple technology demonstration and/or scientific payloads are being considered. [7]

The first possible payload focuses on testing the E-Sail technology for de-orbiting purposes [8]. The experiment would consist of deploying a 300 m long tether and charging it negatively. The ionospheric plasma surrounding the Earth would interact with the generated electrical field and decelerate the satellite. It is most likely that this payload will be included in the satellite. The payload would be jointly developed by the Finnish Meteorological Institute and Tartu Observatory. [7]

The second option being considered is a remote sensing payload that would be developed by Tartu Observatory. The main aim of the payload would be to capture images of the Earth in multiple specific spectral regions for scientific purposes. Due to this being a recent development, the specifics of the system are still under study. [7]

The third payload under evaluation is a high-speed communication system being developed by Ventspils University College in Latvia. The system would communicate in the C-band and be capable of data rates higher than 1 Mbps [9]. Should the remote sensing payload be included in the satellite, the high-speed communication system would complement it very nicely by allowing more images to be transferred.

The final payload under study at the moment is an optical communication system. This system would be used to transfer data from space to ground in a unidirectional manner. A feasibility study is currently being conducted by a research group in the University of Tartu. [7]

2.2. OVERVIEW OF OTHER ELECTRICAL POWER SYSTEMS

Developments in the field of CubeSat electrical power systems, up to the spring of 2013, were given in the author's Bachelor's thesis [10]. Since then, to the author's best knowledge, no significant achievements have been published in terms of EPS design, but there have been some interesting works nonetheless.

It is the author's belief that many satellite teams choose to buy the EPS from a commercial provider rather than design one of their own. This is very sensible, if the commercial products fulfil the needs of the mission. Generally, it seems that EPSs are custom-developed either to meet specific design requirements [11] [12] that the commercial products cannot satisfy, or test new technologies [13] [14]. Both aforementioned practices are also often combined with thesis works [15] [16] [17]. It would be very interesting to study the implementations of the commercial systems, but unfortunately no detailed documentation is available.

2.3. LESSONS LEARNED FROM ESTCUBE-1 EPS

In general, the electrical power system [18] on-board ESTCube-1 worked very well and exceeded the designers' expectations in multiple aspects. Electronics of the EPS worked without failure and no significant degradation was observed during the day-to-day operations. Although the EPS's electronics performed very well, the satellite eventually stopped working due to a lack of sufficient energy production. A very significant drop in the energy harvested was observed over the two years in orbit – it was most likely caused by the severe degradation of the solar panels. It is suspected that the problem was caused by the lack of cover glasses on the cells. Unfortunately, the output voltage and current of the individual solar cells were not measured, as this data would have provided very interesting insight into the degradation process. [19] [20]

In terms of novel solutions, SPV1040 (ST Microelectronics) based energy harvesting system [18] was successfully tested in orbit at spin rates up to 840 degrees per second [19] without any noticeable drop in energy production.

A firmware update system was implemented for the EPS along with the other systems [19]. This proved to be a very useful feature as it helped to fix some critical bugs, add features and reduce power consumption significantly in the later stages of the mission. A similar system is also planned for the next generation of the EPS.

For more in-depth information about the design and results of the ESTCube-1 EPS, see [18] [10] [21] [20] [19].

2.4. SPACE ENVIRONMENT HAZARDS

Designing a system that is intended to function in space is not an easy task by any means. The instrument has to tolerate heavy mechanical loads during launch, only to end up in a hostile environment. As the system is subjected to vacuum, periodic thermal cycles and cosmic radiation, it is very probable that these harsh conditions will degrade both mechanical and electrical systems over time.

Thermal convection is not a viable option for heat transfer in a vacuum environment. The only practical way to transfer heat on the component level is conduction. This, however, only displaces the energy and eventually the excess energy would have to be radiated away as thermal radiation. As off-the-shelf electronic components are thermally designed to be used in environments with close to standard ambient temperature and pressure, more thought has to be put into the thermal design while using these components. One way to mitigate this issue is to use thermally enhanced packages, which feature special thermal pad(s) underneath the devices, meant for conducting heat into the printed circuit board (PCB). It is also very important to ensure a good thermal contact between the circuit board and the rest of the satellite, most importantly, the structure itself.

Periodic thermal fluctuations (thermal cycles) cause expansions and contractions in the components used on-board the satellite. This process can be especially degrading to the solder joints and might eventually produce cracks in them [22]. Proper assembly equipment and methods have to be used in order to produce high quality solder joints that would be less susceptible to this kind of fatigue [23].

Radiation can have degrading or damaging effects on electronics. The parameters of electronic parts may drift due to long term radiation exposure – as the total ionizing dose (TID) increases, the performance of the device usually decreases. Degraded performance may present itself in many different ways, ranging from an increase in power consumption and/or dissipation, to shift in the voltage levels corresponding to logic states. Yearly TID is highly dependent on the orbit parameters, solar activity and satellite construction, and is practically impossible to precisely estimate beforehand [24] [25]. Damage to the satellite caused by TID can be reduced by shielding the critical components [26]. Aluminium is very widely used for shielding, as it is often already being used as the main structural material.

While TID degrades the system over time, the single event upsets (SEU), single event latch-ups (SEL) and single event burnouts (SEB) can cause damage to the system instantaneously. These effects are caused by heavy ions, protons and neutrons. SEUs can cause flipped bits and data corruption, and they are statistically guaranteed to happen in devices susceptible to them [27]. The SELs can cause excessive current consumption due to short circuits inside the device. This problem mainly affects devices that use complementary metal oxide semiconductors (CMOS) [27]. It is usually possible to recover from the aforementioned effects by power-cycling the affected device. The SEB events, by definition, cause permanent, irreversible damage to the affected device. While shielding may be effective for mitigating TID effects, it has minimal impact on reducing single event rates. These effects can only be mitigated by making the system more redundant, more robust and by adding latch-up protection systems. [24] [25] [28]

If possible, it is always recommended to use components that have been subjected to radiation testing. The National Aeronautics and Space Administration (NASA) has a freely accessible database that contains radiation tolerance testing results of various electronic components they have tested over the past 25 years [29].

2.4.1. COMPONENT DE-RATING

The electronic components used in space applications are almost always de-rated in order to improve their reliability. Table 1 has been composed based on the ECSS-Q-ST-30-11C [30] de-rating guidelines and summarizes the suggested de-rating levels for the components relevant to the system being developed.

TABLE 1. RECOMMENDED DE-RATING OF PARAMETERS BASED ON ECSS-Q-ST-30-11C REVISION 1

Component type	Recommended operating level of the maximum
Capacitors (ceramic / tantalum)	Voltage 60%
Feedthrough capacitor	Voltage 50%
Inductors	Voltage 50%
Resistors	Power 50% Voltage 80%
Diodes	Current 75% Reverse voltage 75% Power dissipation 50%
Field-effect transistors (FET)	Drain-source voltage 80% Gate-source voltage 75% Drain current 75% Power dissipation 65%
Power related integrated devices	Supply voltage 90% Applied voltage 90% Output current 80%

3. SYSTEM ARCHITECTURE

3.1. SATELLITE ARCHITECTURE

ESTCube-2 will be using a very different approach to the system's architecture when compared to most CubeSats. A tightly integrated bus is envisioned instead of the more traditional board-per-subsystem approach. The aim is to integrate the critical systems of the satellite very tightly in order to be more volume efficient. Currently, the aim is to compact all the functionality seen in Figure 1 (except side panel systems) so it would occupy less than 0.5 CubeSat units in volume. That would include two battery packs occupying a total of 0.15 units.

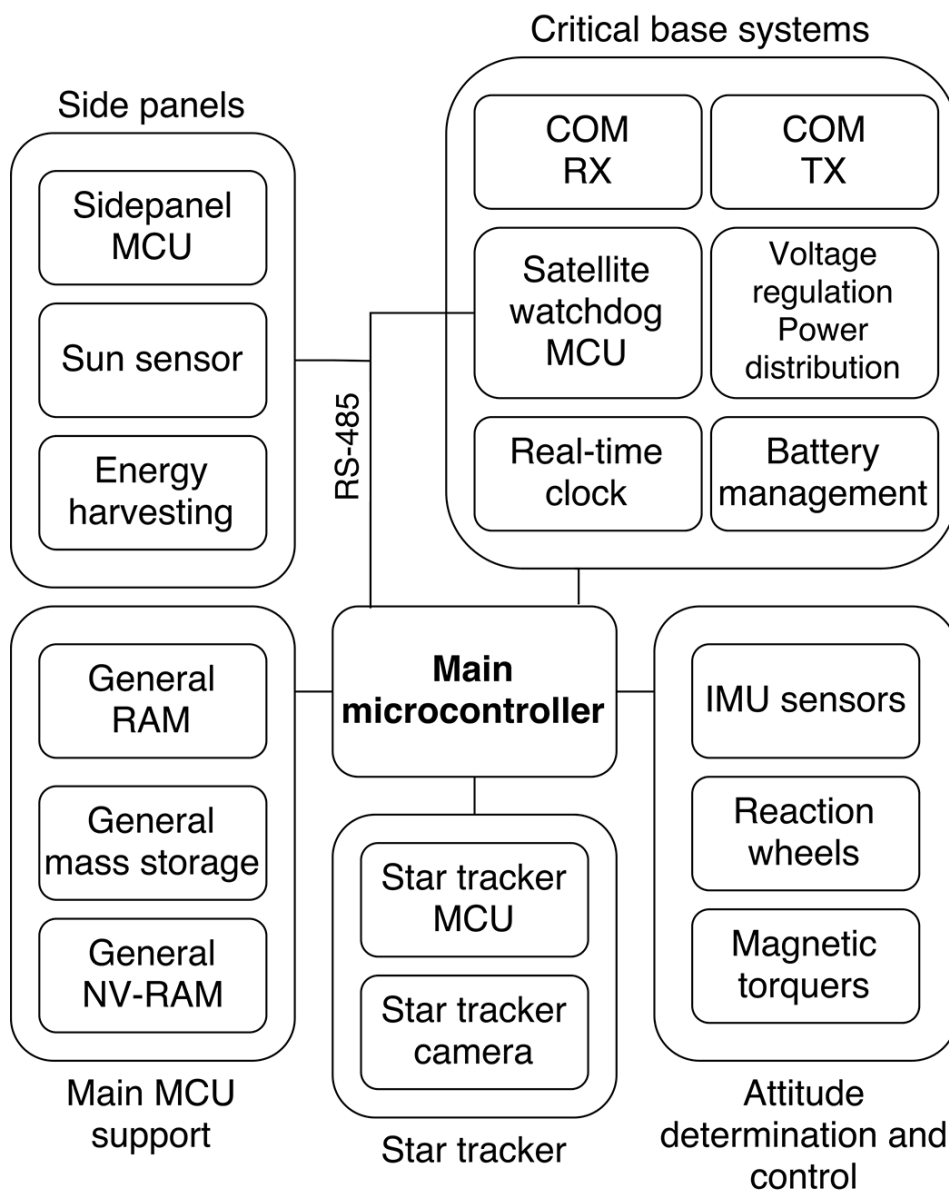


FIGURE 1. SATELLITE'S SYSTEM ARCHITECTURE OVERVIEW. PAYLOADS ARE EXTERNAL TO THE SYSTEM

One very important change concerning the satellite's power distribution architecture is that the regulated voltage(s) will be only provided to the bus in contrast to the whole system, including payloads, as it was in the case of ESTCube-1. The floating battery bus (6.6–8.4 V) will be made available for the payloads through individual current-limited switches. This makes more sense as the satellite has increased in size and it is not reasonable to distribute regulated voltages throughout the satellite due to the voltage drops and power losses caused by the long conductors. This approach also allows more flexibility in terms of payloads because the current available is only limited by the battery discharge protection circuitry and current-limited switches, and not by the voltage conversion stage. In addition, every payload can optimise the converters for its own needs, should it be adjustable output voltage, high efficiency, low output ripple, low electromagnetic emissions or something else. Figure 2 shows a concept of the bus.

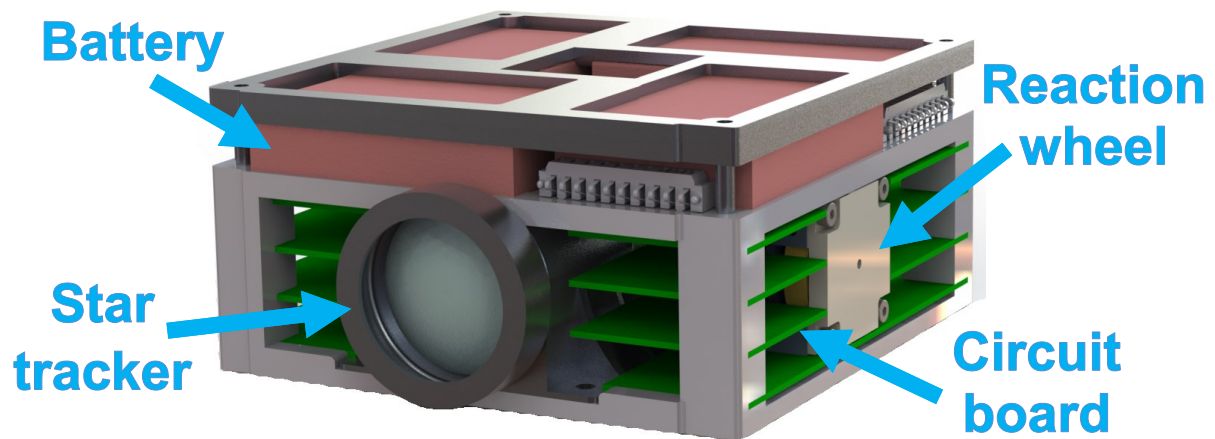


FIGURE 2. COMPUTER RENDER OF A PROPOSED SOLUTION FOR THE BUS (CREDIT: IAROSLAV IAKUBIVSKYI)

3.2. EPS BLOCK DIAGRAM

The EPS consists of four main blocks: energy harvesting, energy storage, voltage conversion and power distribution, and a microcontroller for monitoring and control. The system is centred around the main power bus (MPB), which is a battery-stabilised floating voltage bus. An identical topology was also used on-board ESTCube-1 where it was proven to work remarkably well. Figure 3 shows the block diagram of the system.

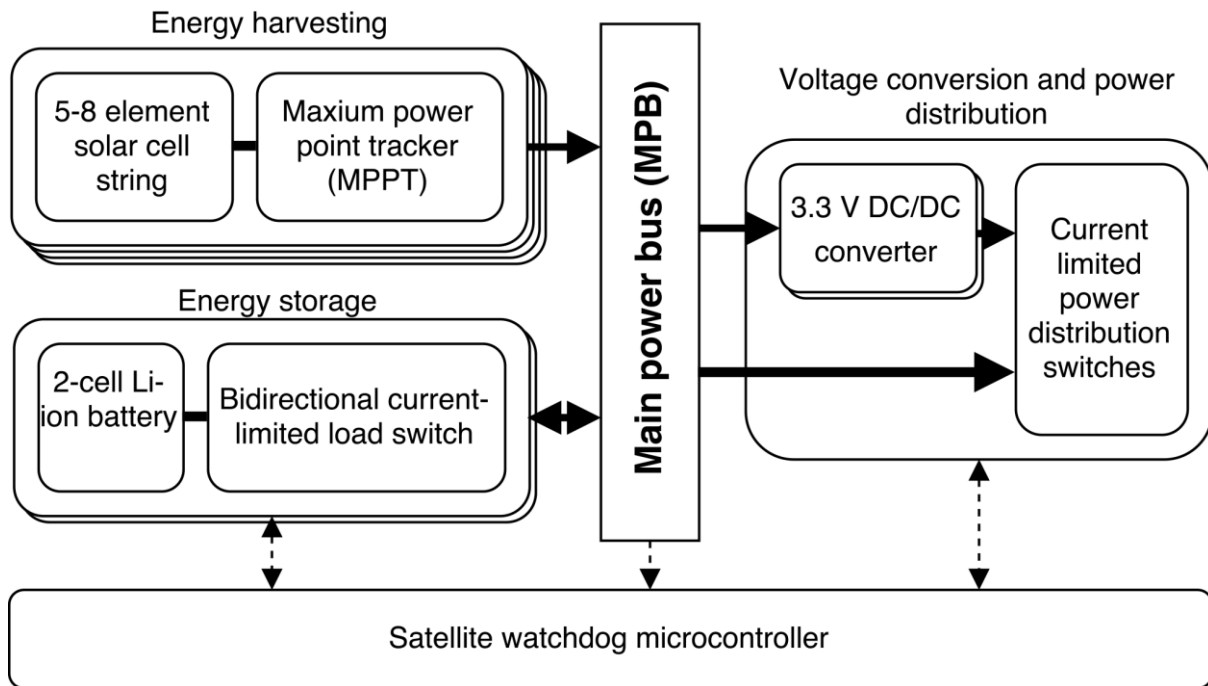


FIGURE 3. ELECTRICAL POWER SYSTEM BLOCK DIAGRAM. THE BOLD ARROWS REPRESENT CURRENT FLOW AND DASHED LINES ILLUSTRATE CONTROL AND MEASUREMENT INTERFACES.

The energy harvesting circuitry will be an independent system mounted on the side panels of the satellite. The harvesting system will be autonomous and will provide power to the MPB whenever it is available from the solar panels. As the design will include a reverse voltage protection circuitry, there is essentially no limit to how many of these systems could be connected to the MPB in parallel. As every side panel will have its own energy harvesting circuitry, it also increases the system's reliability and robustness. The maximum power point tracker (MPPT) circuitry will double as a battery charger, so there is no need for a separate battery charging system. Although a prototype has been built, it has not yet been tested.

The energy storage system will be based on two prismatic Lithium-ion cells connected in series. This also defines the voltage of the MPB, which will vary from 6.6 V to 8.4 V. Candidates for the final cells have been chosen, but they have not yet been tested. In this thesis, the battery protection and management system is discussed in detail in chapter 5.

The voltage conversion and power distribution system is the third major block of the EPS. Its task is to provide the satellites bus, described in chapter 3.1, with the required voltages. It also has to provide the unregulated battery bus to the payloads. Analysis and implementation of this system will follow in chapter 6.

The final integral part of the system is the microcontroller (MCU). In the spirit of integrated systems, the same MCU will manage the EPS's subsystems and will also handle the low-speed ultra high frequency (UHF) communications with the ground station(s). The EPS side of the system was prototyped and tested by Martin Pöder while working on his Bachelor's thesis [31], which was co-supervised by the author. The dual-processor system described in that thesis will not be used because a more capable microcontroller with higher input-output pin count has become available since, but the rest of the software and hardware will be used, nonetheless.

3.3. POWER BUDGET ANALYSIS

In order to properly estimate the necessary voltage conversion capacity, a power budget has to be compiled. Table 2 shows the preliminary power budget based on datasheet data and previous experience with similar systems. From these estimated power needs we can derive the rough requirements for the voltage conversion system. Peak power shows the maximum consumption of the system and average power shows the nominal operating power.

TABLE 2. THE PRELIMINARY POWER BUDGET OF ESTCUBE-2 BUS

Consumer	Voltage (V)	Average power (mW)	Peak power (mW)	Notes
EPS / COM	3.3	15	150	Digital segment
COM RF front end	3.3	10	250	
COM power amp.	Battery	NA	3000	
Side panels	3.3	20	150	Total for 4 side panels
On-board computer	3.3	170	850	
Star tracker FPGA	Battery	1500	3000	If FPGA is used
Star tracker M7	3.3	250	1100	If M7 is used
ADCS sensors	3.3	75	200	
Reaction wheels	3.3	660	2550	Total for 3 wheels
Magnetorquers	Battery	TBD	TBD	

From the power budget it can be seen that all systems in the bus will use either 3.3 V or the floating battery bus. This was agreed upon by the subsystem leads in order to minimise the amount of different voltage conversions needed and maximise efficiency within the system. Should a field programmable gate array (FPGA) be used for the star tracker system, a separate power conversion system will be implemented for the exotic voltages required by the device.

To adequately estimate the minimum and maximum loads that the DC/DC converter will be subjected to, operating modes have to be considered. The satellite's bus will have three main operating modes: low power idle, active ADCS control idle and active mission mode involving high accuracy pointing. The first mode will be very basic, with only the EPS and COM enabled, and would be used to keep the satellite in a stand-by mode to conserve power and/or charge batteries. The active ADCS control idle mode will be used when there is a need to maintain the satellite's orientation, for example pointing the deployed solar panels towards the Sun in order to harvest more energy, or to keep a payload pointed in some general direction. The third mode is very similar to the second one in terms of theoretical peak consumption, but all tasks will be run as frequently as possible. For worst case consumption, it is assumed that the star tracker will be based on an ARM M7 processor and powered from the 3.3 V supply.

TABLE 3. SATELLITE BUS OPERATING MODE FOR LEAST POWER CONSUMPTION (LOW POWER IDLE)

Activity	Power consumption (mW)
EPS / COM system active	25
COM RF RX standby	10
Side panels idle	20
Total	55

TABLE 4. SATELLITE BUS OPERATING MODE FOR HIGHEST POWER CONSUMPTION (ACTIVE MISSION MODE)

Activity	Power consumption (mW)
EPS / COM system processor active	25
COM RF RX standby	10
COM RF TX active	250
Three side panels active	15
Single side panel communicating over RS485	150
ADCS sensor measurements	200
ADCS attitude calculations running on OBC	350
Two reaction wheels at 10k RPM	440
Single reaction wheel breaking	850
Star tracker based on an ARM M7	1100
Total	3390

The maximum theoretical consumption, based on the current estimates, is almost 3.4 W. As this is a very preliminary estimation, based on datasheet information and experience with similar systems, it is sensible to add a margin of 20%. This adds 0.68 W to the previous estimate and totals 4.08 W. The power required on the 3.3 V rail amounts to 1.23 A of current. The de-rating guide, described in chapter 2.4.1, for power related integrated circuits suggested that the maximum output current should be 80% of the converter's rated output. This means that converters with maximum current output of 1.53 A and higher should be considered.

4. METHODOLOGY AND MEASUREMENTS

4.1. VOLTAGE CONVERTER PERFORMANCE EVALUATION

Voltage converters can be characterized based on different parameters, such as: conversion efficiency, output voltage stability, output ripple, transient response, radiated emissions, thermal performance, etc.

In the scope of this work, multiple converter candidates were prototyped and evaluated to select the best device for the satellite bus. The selection was based on the test-and-eliminate method.

Following parameters were evaluated or measured:

- Conversion efficiency
- Output voltage stability
- Output voltage ripple
- Transient response
- Near-field electromagnetic emissions
- Number of components required to implement

4.2. BASE TESTING PLATFORM

Measuring DC/DC converter performance manually is a tedious and time consuming process. In order to speed the process up and test multiple different devices through a repeatable process, a testing platform was designed and constructed. The first revision of the platform was designed and built by Karl-Indrek Raudheiding while working on his Bachelor's thesis [32], which was co-supervised by the author. An improved second revision of the platform hardware, used in this work, was designed and assembled by the author and Mr. Raudheiding. The iteration fixed bugs and improved upon the functionality. The block diagram of the measurement platform can be seen in Figure 4 along with the 3D render of the physical system in Figure 5.

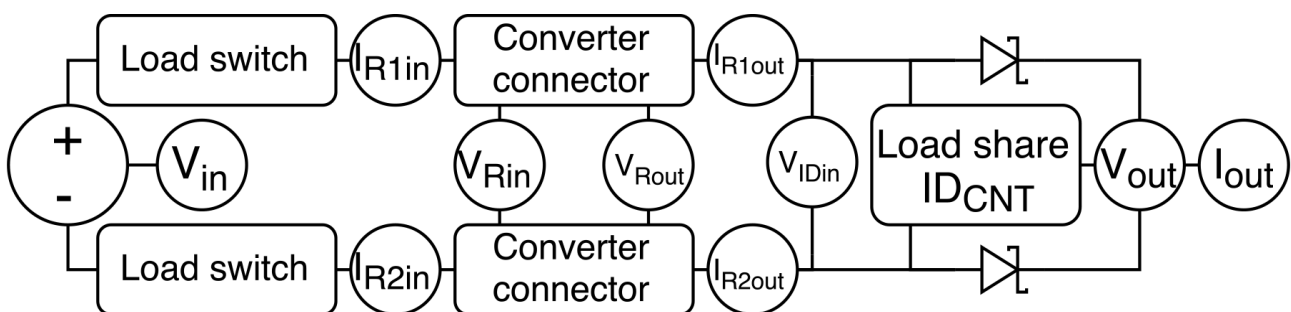


FIGURE 4. BLOCK DIAGRAM OF THE MEASUREMENT PLATFORM

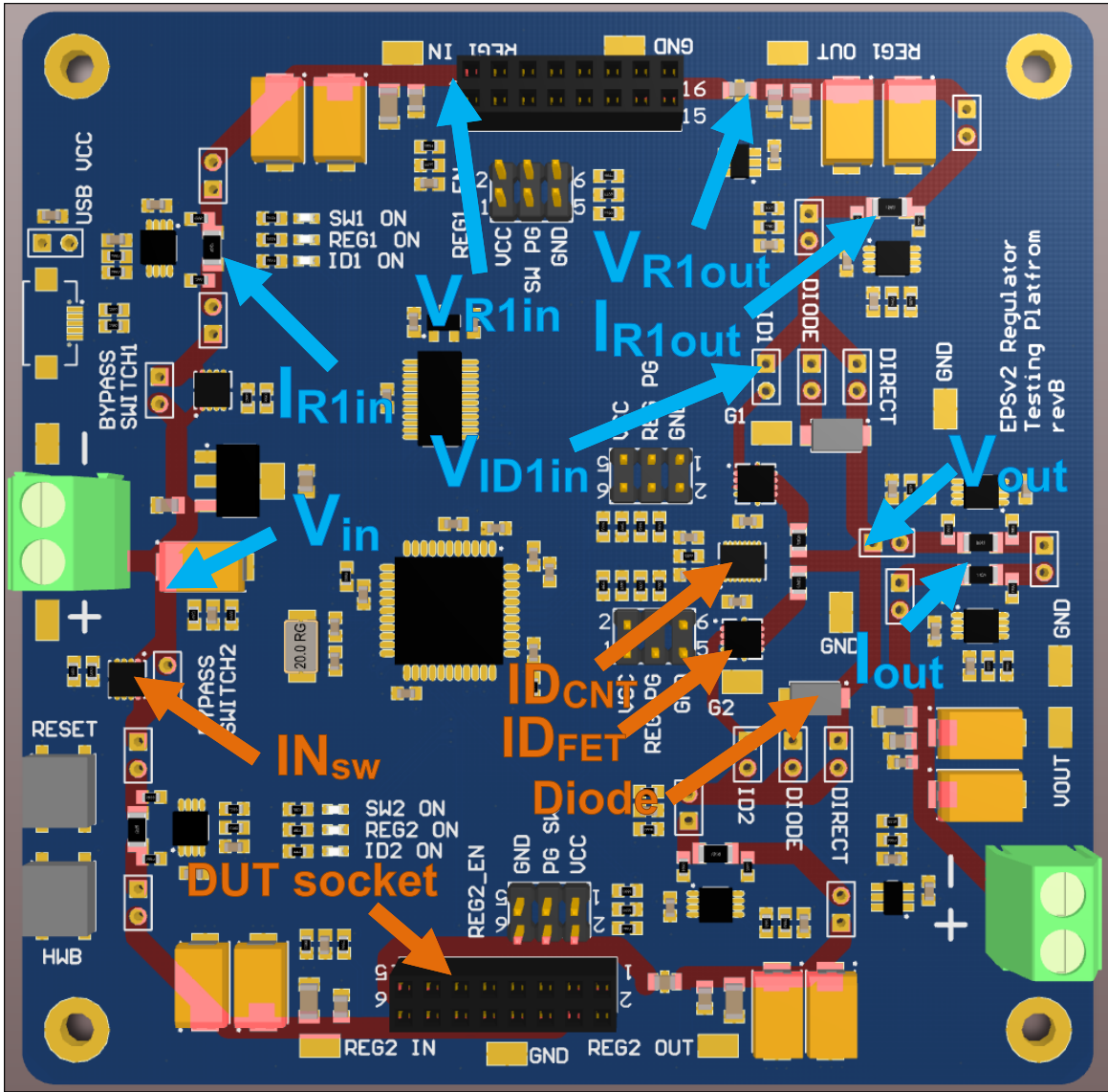


FIGURE 5. COMPUTER RENDER OF THE REGULATOR TESTING PLATFORM WITH CERTAIN DEVICES AND MEASUREMENT LOCATIONS HIGHLIGHTED. THE HIGHLIGHTED DARK RED TRACES SHOW THE PATH OF HIGHER CURRENT THROUGHOUT THE PLATFORM.

The platform was designed to emulate, as closely as possible, the voltage conversion system (described in chapter 6) that would be used on-board the satellite, while also measuring the performance of the devices being investigated. Major parts of the system are the input load switches (I_{Nsw}), the converter module connectors (DUT socket) and the current ORing circuitry (I_{DCNT} , I_{DFET} and Diode). The measurement places for a single channel (I_{R1in} , V_{R1in} , V_{R1out} , I_{R1out} and V_{ID1in}) along with locations common to both channels (V_{IN} , V_{OUT} and I_{OUT}) are highlighted in Figure 5. The measurement locations of the second channel are symmetrical to the first and are not explicitly shown.

These locations were carefully chosen so that the platform specific losses would not affect the final results. There are some additional measurement points for that reason. For example, the converter output voltage (V_{R1out}) is measured along with the input voltage (V_{ID1in}) of the load sharing stage. In the real system, the converter's output current is not measured, thus there are no measurement related losses present. The aforementioned two measurements enable calculating the regulator's efficiency and the output stage losses more precisely.

All measurement points on the platform were calibrated with a DMM4050 6.5 digit benchtop multimeter. Based on the calibration data, a linear regression model was constructed. In order to verify the calibration results, the input and output currents were measured simultaneously with two DMM4050 multimeters and the platform. Based on the two sets of measured results, the conversion efficiencies were calculated. The difference between the two efficiencies was within two percent at lower currents (up to 100 mA) and within one percent for the rest of the measured range.

This system was not only used for the final tests, but was an invaluable tool during the development of the converter candidate modules. The automated operation of the platform enabled rapid development cycles where multiple different component combinations were tested to achieve optimum performance.

4.2.1. CONVERTER EFFICIENCY

The measurement platform was used to automatically measure parameters needed to calculate the converter efficiency: input and output voltage and current. In order to obtain an efficiency curve with a good resolution, the parameters needed were measured after every output current increment of 10 mA. It took approximately 130 seconds to measure a single converter module at a single input voltage at loads up to 1.5 A. After every current increment, ten measurements sets were queried from the measurement platform and averaged in order to get a more precise and stable result. All parameters were measured at three different input voltages based on different battery states: 6.6 V (almost empty), 7.4 V (nominal) and 8.4 V (full).

4.2.2. OUTPUT VOLTAGE RIPPLE

A special adapter containing an AC decoupling capacitor, 50 Ω matching resistor and an SMA connector was soldered onto every DC/DC module output capacitor. This enabled easy and quick connection to the oscilloscope via an SMA cable. Rigol DS1104Z-S oscilloscope with a 20 MHz bandwidth limit was used for this experiment. The setup was recommended in an application note [33] focusing on power converter verification. Figure 6 illustrates the setup.

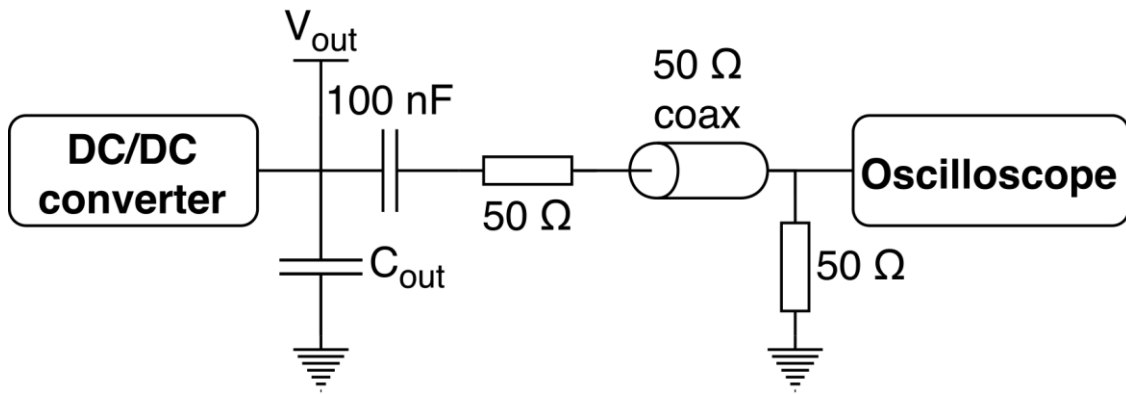


FIGURE 6. RIPPLE MEASUREMENT SETUP

The oscilloscope has software built in to automatically measure parameters of interest, such as peak-to-peak voltage (V_{PP}) and root mean square voltage (V_{RMS}). The oscilloscope has a built-in statistics module capable of averaging measurements over time. Prior to measuring the ripple voltage of the DC/DC converter output, the measuring script reset the statistic module. Measurements were collected for seven seconds before saving the values into the result matrix. The seven second threshold was found empirically by evaluating how fast the average value stabilised.

4.2.3. TRANSIENT RESPONSE

Transient response testing means that the load applied to the converter is changed very rapidly with a large amplitude. Typically, the load is increased from zero (or very small) current to the maximum output current. The slew rate can vary from $0.1 \text{ A}/\mu\text{s}$ to more than $50 \text{ A}/\mu\text{s}$. [34]

A self-built transient tester was used for testing. It consisted of a low $R_{DS(on)}$ N-channel metal oxide semiconductor field-effect transistor (MOSFET) and a gate driver. A wire wound resistor and a rheostat were used as the static loads during testing. The switch was located between the load and the ground return (low side switching). Rising and falling edge slew rates of $7.25 \text{ A}/\mu\text{s}$ were achieved with the device.

4.2.4. NEAR-FIELD ELECTROMAGNETIC EMISSIONS

The near-field electromagnetic emissions were measured at Tartu Observatory with an ETS-Lindgren's near-field probe 7405-903 and a Rohde-Schwarz ESR26 spectrum analyser. All measurements were conducted in peak-hold mode by moving the probe around the device under test (DUT) as close as possible. The accuracy of the measurements should be within 1 dB.

4.2.5. TESTING METHODOLOGY AND DATA ANALYSIS

The measurement platform input was connected to a computer controlled power supply (Rigol DP832) and the output was connected to a programmable electronic load (MightyWatt [35]). This setup, controlled by a MATLAB measurement script developed by the author, enabled performing repeatable automated measurements.

Two DC/DC converter modules were used to measure the performance of each device. Both modules were tested in both channels which amounts to four full measurements (applies to efficiency and ripple results). The similarity of the measurements was verified visually and afterwards the results were averaged to produce one set of results per converter.

Multiple automated analysis scripts were developed by the author. These scripts performed tasks, such as averaging, calculating various parameters and plotting. This setup enabled analysing large amounts of data automatically and provided a quick visual feedback of the results. The scripts were developed in the MATLAB environment.

5. BATTERY MANAGEMENT AND PROTECTION

5.1. REQUIREMENTS

1. The system shall be compatible with the system architecture described in chapter 3.2
2. The system shall be capable of bidirectional and unidirectional operation
3. The system shall be capable of disconnecting batteries from the MPB
4. The system shall be capable of passing 6 A discharge and 1.5 A charge currents in the bidirectional mode
5. Both directions shall have adjustable current limits
6. Auto-resettable fault handling system is preferred
7. Battery cell voltages shall be measured
8. Instantaneous currents shall be measured in both directions
9. The system shall be capable of measuring total charged and discharged energy
10. The system shall have automatic over- and under-voltage protection which can be overridden by the microcontroller
11. It shall be possible to add a system that balances cell voltages (requirement will be revised after battery testing campaign)
12. The quiescent current shall be low enough to ensure a shelf life of one year

5.2. GENERAL SYSTEM DESIGN

As required, the battery system will have to perform three main tasks: switch between charge, discharge and bidirectional modes; provide protection against over- and under-voltage (OV and UV), overcurrent (OC) and cell imbalance scenarios; and collect information about the state and health of the system.

The battery protection side was designed so that it would react to most faults automatically and require no input from any external systems. For every required functionality multiple implementations were considered. The following chapters will describe the operating principles of each subsystem, cover the pros and cons of the alternative solutions and make a recommendation on which solution to use and why.

5.3. BATTERY BALANCING

A battery balancing system is needed in order to balance individual cells in a multi-cell battery pack. Should this issue not be addressed, the cells could go out of balance during the charge-discharge cycles. The imbalance is often caused by the cells having different characteristics at

the beginning of life or due to degradation at different rates. In practice, this means that one cell will end up being at a higher voltage compared to the other one. The battery charging device monitors the total voltage of two cells in series and terminates when the voltage rises to around 8.4 V. This might cause an issue where one cell is being charged to 4.25 V and the other one to only 4.15 V. Should the cells not be balanced by an external system, an auto-accelerating degradation cycle may begin with the voltage differences rising over time. Lithium-ion batteries are very sensitive to over-voltage conditions and can be damaged permanently, if those conditions persist. In extreme cases the batteries may rupture or even explode. [36]

It has to be noted that some CubeSats using two cells in series have not implemented battery balancing at all [11]. In this work the balancing system is covered, but battery testing will show, whether it is ultimately needed or not.

The simplest controlled balancing system consists of a switch and a resistor. With this method, it is possible to discharge the battery on demand with a very low current and drain the cell with the higher voltage enough to achieve balance between the cells. The obvious disadvantage of this system is that the discharged energy is turned into heat and wasted.

Alternatively a charge redistribution system could be used that transfers energy from one cell to another. These systems are usually based on capacitive or inductive components and are much more complicated to operate and implement [36]. These systems were not considered due to their complexity.

Two solutions for the final implementation were considered: a BQ29209 (Texas Instruments) battery balancer based system and an MCU controlled balancing system.

The former would require some external components in order to function, but it would not require any additional software development other than turning the balancer on and off. As the logic is integrated into the device, it would turn off automatically after balance has been achieved. This system has the required voltage sensing functionality integrated and would only require an enable signal (single IO pin) from the controller. As the rated supply current for the balancer is very low (6 μA) in standby, it might also be feasible to enable the device permanently and not commit any IO pins at all. This however, requires further analysis as it would not be possible to turn the device off and might introduce an additional failure mode.

The MCU based solution would require adding load resistors and switch transistors to the system. Since the cell voltage sensing system is required anyway, there is no need for extra

sensing functionality. The biggest downside is that it would be necessary to develop and test additional software in order to achieve the required functionality. Furthermore, two IOs per battery pack would be required to control the balancers.

The author's recommendation is to use the BQ29209 based system due to implementation simplicity and the minimal amount of software development and testing required.

5.4. UNDER- AND OVERVOLTAGE PROTECTION

Lithium-ion battery cells are very sensitive to excessive discharging and overcharging. For this reason, it is critical that the system includes protection schemes from under- and overvoltage conditions. Without this functionality, there is a risk of damaging the battery elements permanently.

On ESTCube-1, this system was not implemented in hardware and the task was performed by the software. The system worked and also provided the operators with the flexibility of changing the UV/OV thresholds on the fly. The adjusting functionality was used in the last stage of satellite operation in order to allow for deeper discharge cycles. This approach, however, introduced additional complexity to the software and relied on the analog-digital converters (ADC) for measurement data.

For the next generation system, automatic hardware level implementation with a microcontroller override functionality is desired. Originally, two solutions were considered: TPS3700 (Texas Instruments) window comparator based system and a custom implementation based on discrete Schmitt triggers (essentially building the window comparator from scratch). However, after some investigations into the custom implementation were done, the idea was dropped. The only benefit would have been customisable hysteresis. In all other aspects (expected quiescent current, component count and PCB footprint, amount of time required to implement and test) the TPS3700 outperformed the discrete solution. Based on these arguments, the author made the decision not to proceed with further investigations into the custom design and decided to use the TPS3700.

5.5. LOAD SWITCH DESIGN

The main requirement for the system is that it must be capable of switching the charge and discharge paths on and off. The system must also be switched off when the current limit is exceeded (possibly with auto-reset functionality). On ESTCube-1 the problem was solved with two TPS2557 (Texas Instruments) load switches in a special back-to-back configuration [18].

As that system was rated up to 5 V and 2 A, it was not possible to use the legacy implementation and a new system was needed.

The proposed load switch designs are based on hot-swap controllers. These devices are originally designed to be used in systems which incorporate hot-swappable modules, such as data storage systems, servers, telecom equipment, etc. Our system does not include any hot-swappable modules, but we require very similar functionality. The controllers themselves are capable of driving external power MOSFETs and also provide automatic current-limiting and circuit breaker functionality with configurable activation and cooldown delays. The ability to choose external power switch components enables the use of very low-loss devices, such as SiA04DN (Vishay) power MOSFETS. They feature very low $R_{\text{DS(on)}}$ of only $2\text{m}\Omega$ at $10\text{ V } V_{\text{GS}}$, high current capacity and a compact surface mount package with enhanced thermal contact. The automatic current-limiting and circuit breaker functionality is tied to the voltage drop on the shunt resistors. Unfortunately, the aforementioned functionalities will be triggered on fixed voltage drops and therefore the limits can only be configured with different shunt resistor values. Should asymmetric current limits be needed, two different shunts have to be used. Both hot-swap controllers have pin-compatible versions with either latch-off or automatic reset fault handling capability.

The following paragraphs mention the term “ideal diode”. As they do not exist in real life, some elaboration is required. Controllers, which actively drive a MOSFET in order to achieve a diode-like behaviour, are called ideal diodes. The FET is driven to a voltage drop of around 20 mV until the natural voltage drop due to the $R_{\text{DS(on)}}$ takes over. [37]

5.5.1. LTC4226 BASED DESIGN

The first proposed design is based on LTC4226 (Linear Technology) hot-swap controller which is originally meant to be used in a dual current path system, but is also capable of working with the MOSFETs in a back-to-back configuration. The specific configuration of the FETs is required in order to prevent current flow between the MPB and the battery pack through the body diodes when both FETs are turned off. Figure 7 demonstrates the configuration.

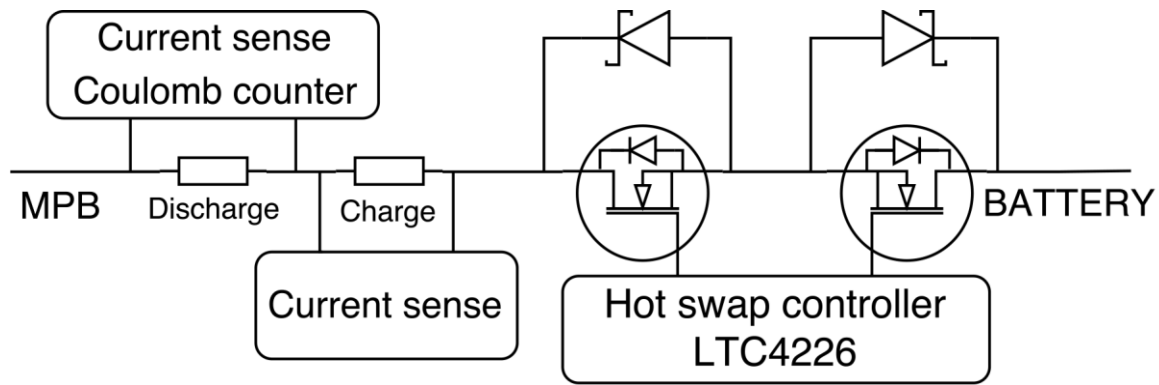


FIGURE 7. LTC4226 BASED BATTERY SWITCH. NOTE: THE DIAGRAM ONLY ILLUSTRATES THE MOST CRITICAL CONNECTIONS NEEDED FOR UNDERSTANDING THE OPERATION OF THE SYSTEM. THE PHYSICAL IMPLEMENTATION IS MORE COMPLEX.

The bidirectional current flow requirement is achieved easily when both FETs are turned on. If one of the switches is turned off, the current will unidirectionally flow through the diode paralleled with the other switch. This solution, however, comes with obvious drawbacks: some of the power is dissipated on the diode and the voltage on the other side of the diode is also significantly lower. A similar system for the unidirectional operation was used on-board ESTCube-1. The unidirectional mode will not be used during normal operations and will only be activated under special conditions, therefore these drawbacks are not considered to be major.

The circuit breaker and current limiting functionalities are dependent on the voltage drop on the shunt resistor. If the voltage drop exceeds 50 ± 5 mV, the device starts charging an external fault capacitor with a constant current. If the voltage drop reaches 86 ± 16 mV, the device enters active current limiting mode in which the excessive energy is dissipated on the external FET. When the device is in current limiting mode, the fault capacitor is charged with a larger current. When the fault capacitor reaches a certain voltage level, the device turns off. There are two versions of the device available that differ in the way they handle faults. The latch-up version of the device remains off, but the auto-reset version starts a 0.5 second timer and tries to turn on, after it expires.

The battery protection system is required to have a shelf life of at least a year because launches are often postponed and the satellite might have to be in storage for an extended period of time. This requirement makes the quiescent current very important. The controller is not directly connected to the battery side, so there is no direct current flow. This might make it possible to avoid having a separate switch between the system and the battery. This topic is further covered in the testing chapter.

This implementation has one major downside: the current limit has fixed voltage drop thresholds, so if asymmetrical limiting is required, it is not possible to use the same resistor for both directions. As the requirement is 1.5 A for charge and 6 A for discharge, the charge resistor has four times the resistance of the discharge shunt. Simple calculations show that the resistance values should be 8 m Ω for discharge and 33 m Ω for charge. As the current goes through both resistors, the worst case voltage drop at 6 A discharge would be in the order of 250 mV. In this scenario, 300 mW would be dissipated on the discharge shunt and 1.2 W on the charge shunt. The de-rating guide specifies 50% power de-rating for resistors, meaning that the resistor should be rated for more than 600 mW and 2.4 W, respectively. Such resistors are available, but they are quite large relative to other components. The author had an idea to bypass the charge resistor with an ideal diode, but the idea was discarded after further consideration due to added complexity.

As the switch design already includes shunts for the circuit breaker functionality, there is no need to add additional resistors for the required diagnostic purposes. INA210 (Texas Instruments) and INA213 (Texas Instruments) current sense amplifiers (CSA) and LTC4150 (Linear Technology) Coulomb counter were chosen to perform the tasks. All the previously mentioned devices are capable of bidirectional operation. The INA210, which has a gain of 200 V/V and ultralow input offset voltage of 0.55 μ V typical and 35 μ V max, would be used with the higher value shunt to enable accurate measurements in the lower current range. The ultra low V_{OS} ensures that the maximum offset in terms of current would be around 1 mA. After that device saturates at around 220 mA, the INA213 would be used with the discharge shunt to measure the higher currents. As the latter device has much larger V_{OS} , the accuracy of the results would not be as good. However, if needed, the offset voltage could be calibrated between the two devices on-the-fly at the current range common to both devices enabling accurate results at higher currents with extrapolation. This holds true only if the offset voltage is constant over the whole range. As a 12-bit analog-digital converter with a 3 V reference will be used to digitize the results, the expected resolution for the lower range is 100 μ A/bit and 1.8 mA/bit for the higher range. The Coulomb counter has impulse and direction outputs which are very easy to monitor digitally. The counter is connected to the shunt with a lower value to limit the maximum V_{SENSE} voltage on the shunt to 50 mV. Calculations based on the datasheet show that each impulse would correspond to 1.07 mAh of energy transferred.

Typical gate-source voltage of the driver is 12 V and is rated to maximum of 16 V. As the SiA04DN gate-source voltage is rated to 20 V, the maximum of 16 V slightly exceeds the suggested 75% de-rating threshold. This is considered to be acceptable.

5.5.2. LTC4228 BASED DESIGN

The second design is based on LTC4228 (Linear Technology), which is a dual channel ideal diode hot-swap controller and is similar in functionality to LTC4226 discussed earlier, but it has some key differences. Figure 8 illustrates the second solution.

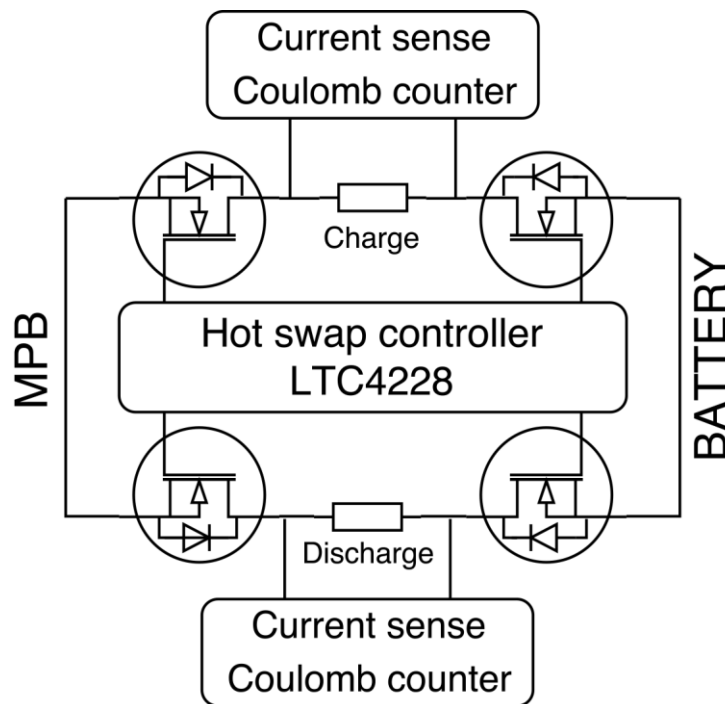


FIGURE 8. LTC4228 BASED BATTERY SWITCH. NOTE: THE DIAGRAM ONLY ILLUSTRATES THE MOST CRITICAL CONNECTIONS NEEDED FOR UNDERSTANDING THE OPERATION OF THE SYSTEM. THE PHYSICAL IMPLEMENTATION IS MORE COMPLEX.

The first difference is that it utilizes ideal diodes (driven MOSFETs) in order to make the current path unidirectional. The second key difference is that it is possible to use one channel for charge and the other one for discharge. As they are both unidirectional, there is no reason to worry about reverse currents. The third difference is that the shunt resistors for circuit breaker functionality are not connected inline and the losses inherent to the LTC4226 based design are not present. This means that this design is much more efficient under higher loads.

The circuit breaker and current limiting functionality is similar to the LTC4226, but LTC4228 features more accurate tolerances for the protection activation thresholds (50 ± 2.5 mV for circuit breaker and 65 ± 10 mV for current limit). The auto reset version does not have a fixed delay

but, the delay is tied to the fault capacitor capacitance. The cooldown delay is approximately 916 times longer than the circuit breaker delay.

The major downside of this design is its current draw. The device needs direct connections to the battery bus and consumes current through those connections. The input current is rated to 2.5 mA typical and 5 mA maximum, additionally the shunt voltage sensing pins together can draw up to 600 μ A. Due to the high current requirements, an additional switchable element is required between the battery terminals and the battery bus in order to meet the shelf life requirement.

As the current flows through the shunts in one direction, bidirectional sensing is not required. Sensing the instantaneous current at the charge pin is not very complicated due to the limited dynamic range required. LT6102 (Linear Technology) CSA features adjustable gain and very low V_{OS} (3 μ V typical and 35 μ V maximum). If the gain is set to 60 and a 12-bit ADC with a 3 V reference is used, the charge current could be measured with a resolution of 0.37 mA/bit. The discharge current measurement is more complicated as the dynamic range is much larger. One option would be to use the LT6102 with adjustable gain and use larger gain for smaller currents and *vice versa*. The gain switching could be accomplished with a simple FET and a resistor in parallel with the static gain resistor. Gain of 60 could be used for higher range (up to 6 A) and gain of 250 for lower range (up to 1.5 A). This configuration would result in resolutions of 1.5 mA/bit and 0.37 mA/bit. As there is no common resistor for both current paths, two Coulomb counters would have to be used. LT4150 would be sufficient for the task.

The nominal output gate-source voltage is rated to 12 V and to a maximum of 14 V. As the SiA04DN gate-source voltage is rated to 20 V, the maximum of 14 V is just under the suggested 75% de-rating threshold.

Only dual channel hot-swap controllers were considered for this system because they enabled a simpler and a more compact solution. Also, based on the datasheets of the single channel devices, no immediate benefits were seen that could justify the increased investment into development, both time- and funding-wise.

5.6. TESTING RESULTS

Both load-switch architectures were tested: voltage drop was measured over the full operational current range in all operating modes (uni- and bidirectional charge and discharge) at three different voltages along with the quiescent current. The voltage was measured as close to the input and output of the switch as possible in order to minimize the losses caused by the

prototype PCB design. In bidirectional mode, both directions were enabled simultaneously and in the unidirectional mode, one of the directions was forced off.

First, the dependency between the voltage drop and the applied voltage was investigated. The performance was measured over the full current range at three different voltages: 6.6, 7.4 and 8.4 V. The worst case standard deviation in bidirectional mode was 580 μV for LTC4226 and 490 μV for LTC4228; in unidirectional mode, 2.08 mV for LTC4226 and 260 μV for LTC4228. These results show that the voltage drop is effectively independent of the applied voltage.

Figure 9 and Figure 10 illustrate the losses of the two topologies dependent on the operation mode: either unidirectional or bidirectional. As LTC4228 proved to be independent of the operating mode during testing, it is only plotted once. The figures show the loss in percentage from the total energy passed. Higher losses are present at lower voltages.

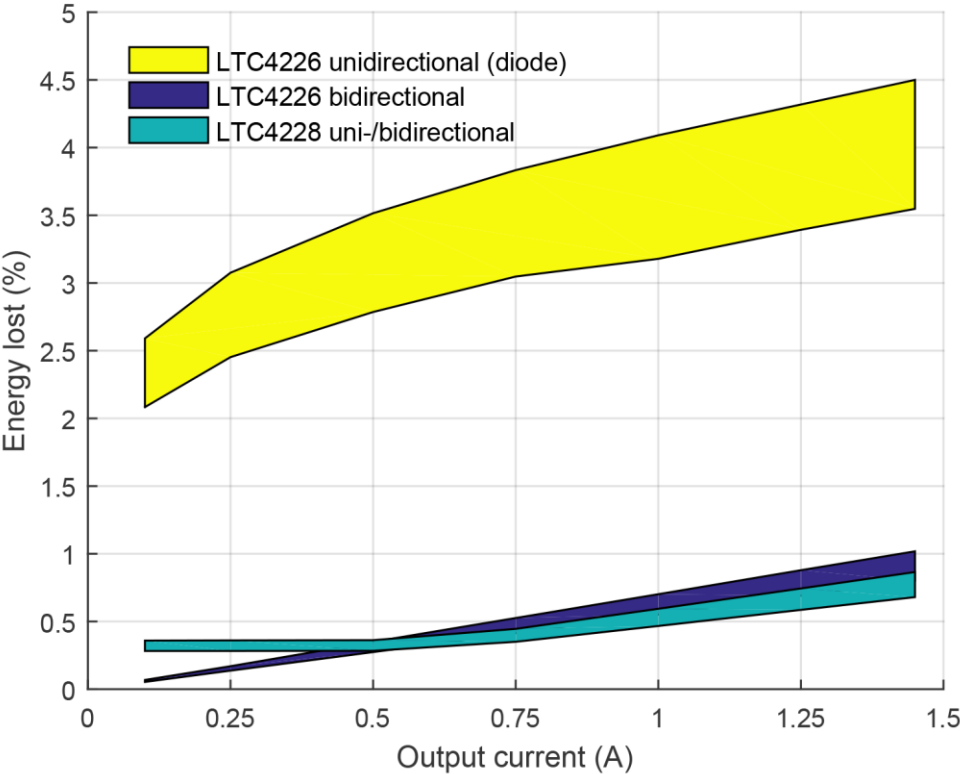


FIGURE 9. CHARGE MODE LOSSES OF POWER SWITCHES. THE THICK LINES SHOW THE LOSSES BETWEEN VOLTAGES OF 6.6 AND 8.4 V

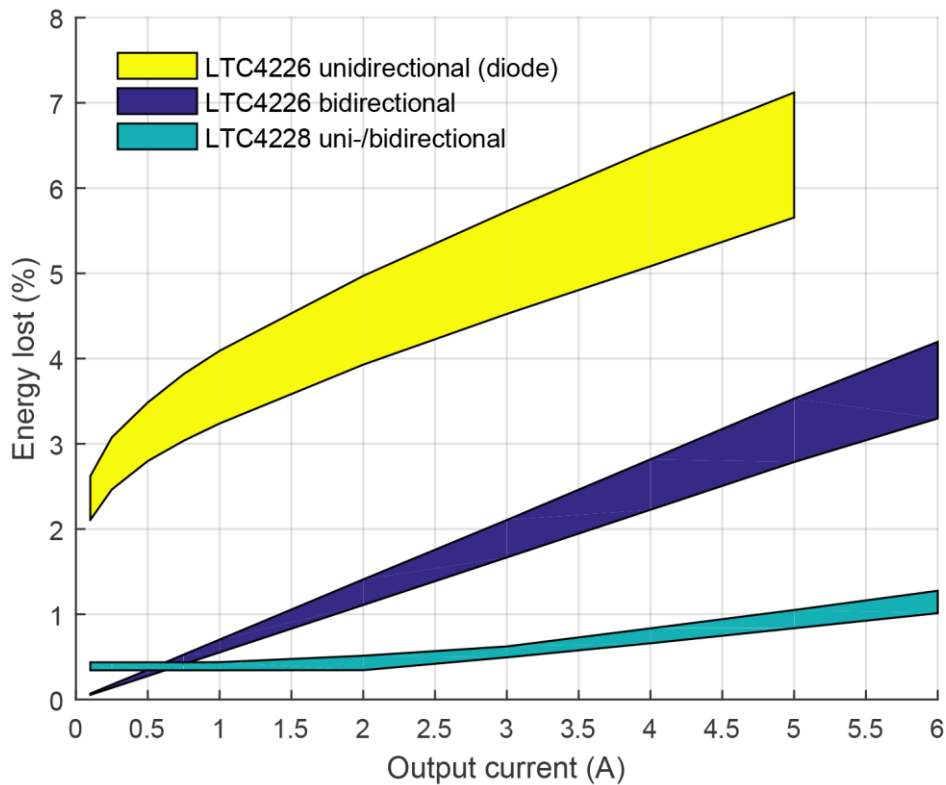


FIGURE 10. DISCHARGE MODE LOSSES OF POWER SWITCHES. THE THICK LINES SHOW THE LOSSES BETWEEN VOLTAGES OF 6.6 AND 8.4 V

In the LTC4226 based solution, PMEG3050 (NXP) low-dropout Schottky diodes were used in parallel with the MOSFETs to divert the current flow from the FET body diodes in the unidirectional operation mode. The diodes are rated to a continuous current of 5 A and to a power dissipation of 625 mW with the standard footprint. If the derating recommendations are respected, the maximum current is limited to around 1 A due to the 50% de-rating regarding the power dissipation. During testing, the diodes were subjected to the maximum rated current for the sake of the argument.

The testing results, unsurprisingly, confirm what was discussed in the design section. While the difference in losses is not substantial during battery charging, the difference becomes quite large for discharge, especially at higher currents. Efficiency wise, the LTC4228 based system noticeably outperforms the LTC4226 based system.

In order to meet the shelf life requirement of one year, the constant load current has to remain below $140^1 \mu\text{A}$. The quiescent current was measured for both prototypes: LTC4226 with the

¹ Calculation based on a fully charged battery with 1800 mAh of capacity and depth of discharge of 70%

PMEG3050 diodes drew 0.73 mA and the LTC4228 drew 4.1 mA when turned as off as possible (it is not possible to turn off the internal voltage regulator). However, when the PMEG3050 diode was removed, only 34 μ A was drawn by the LTC4226. As the current draw of this system is mainly dominated by the reverse leakage of the diode and should the diode be replaced with another featuring lower reverse currents, the system should meet the shelf life requirement without any additional hardware. The LTC4228 based system would definitely require an additional switch to meet the shelf life requirement. It is not possible to reduce the power consumption in any other way without impacting the functionality of the device. The addition of components into this critical current path would of course reduce reliability and increase complexity.

The experience with the ESTCube-1 battery system showed that the unidirectional mode was used under special circumstances once or twice during the two years of operations and the rest of the time the system was operating in the bidirectional mode. The author believes that this will also be the case with the system under consideration and the unidirectional operation mode will be used seldom, if at all.

The 6 A discharge current requirement was set considering the worst possible case: only one battery pack is functional and the bus systems plus a high current consumption payload have to function at the same time. In reality, the satellite is very likely to include at least two battery packs for redundancy and under nominal conditions both of these packs would be turned on, thus a single pack would provide only half of the consumed current. This means that under nominal operating conditions the difference in the losses between the two proposed solutions would be quite insignificant in terms of the whole system.

Based on the previous discussion, the author would recommend the LTC4226 based system for the final implementation. Although the losses inherent to this system are considerably higher at larger currents, the possibility to use it without any additional power switching circuitry and meet the shelf life requirements outweighs the drawbacks. Fewer components mean higher robustness and reliability.

6. VOLTAGE CONVERSION AND POWER DISTRIBUTION

6.1. REQUIREMENTS

The voltage conversion circuit design shall meet the following requirements:

1. Shall provide a regulated output voltage of 3.3 V
2. The input stage and converters shall operate from 6.6 V to 8.4 V
3. Shall be capable of providing output current of at least 1.5 A
4. The converter shall be protected against excessive current draw
5. It shall be possible to measure input instantaneous current
6. Output voltage stability shall be better than ± 50 mV over the full output current range
7. The converter shall operate efficiently ($>80\%$) in the discontinuous mode
8. The system shall be of redundant design consisting of two independent regulators capable of operating in hot and cold redundant modes
9. The converter shall be in a thermally enhanced package
10. The system shall be designed with high efficiency and low losses in mind

The power distribution system shall meet the following requirements:

1. The system shall be capable of operating at voltages up to 9.5 V
2. The system shall be capable of operating at currents up to 3 A
3. It shall be possible to switch loads on and off
4. There shall be an overcurrent protection circuit with an adjustable limit for each load
5. It shall be possible to configure the system to latch-off or auto-reset with a delay
6. It shall be possible to measure output instantaneous output voltage and current

6.1.1. VOLTAGE CONVERSION SYSTEM DESIGN

The voltage conversion system consists of three sequential stages: input load switch and current measurement, voltage conversion, and load sharing system. The last stage has to OR together the converter outputs into a single regulated voltage rail. Two separate conversion channels are implemented for redundancy. All of the aforementioned functionalities will be covered in the chapters to follow. Figure 11 illustrates the system.

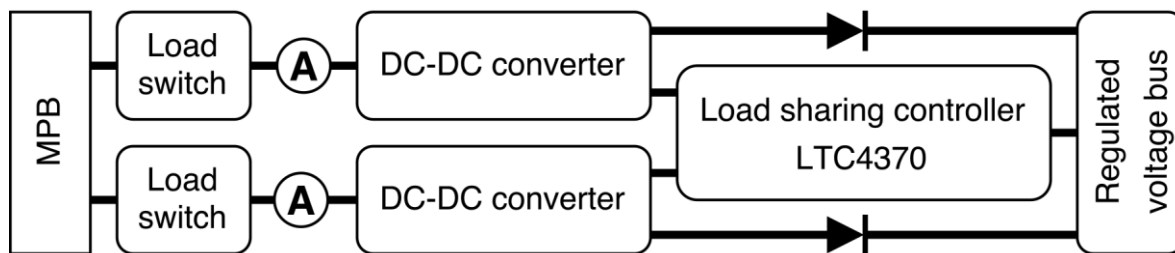


FIGURE 11. VOLTAGE CONVERSION SYSTEM DIAGRAM

6.2. CONVERSION INPUT STAGE DESIGN

Three functionalities are required from the voltage conversion system input stage: ability to switch input current on and off, protection from excessive input current, and instantaneous current measurement capability.

Two input switch designs were chosen for evaluation: a FPF2700 (Fairchild) load switch based and an ADM1170 (Analog Devices) hot-swap controller based. The main difference between them is that the load switch is a fully integrated device with internal current sensing and switching FET while the hot-swap controller based system features an external current sensing shunt resistor and an external MOSFET for load switching. Figure 12 illustrates both implementations.

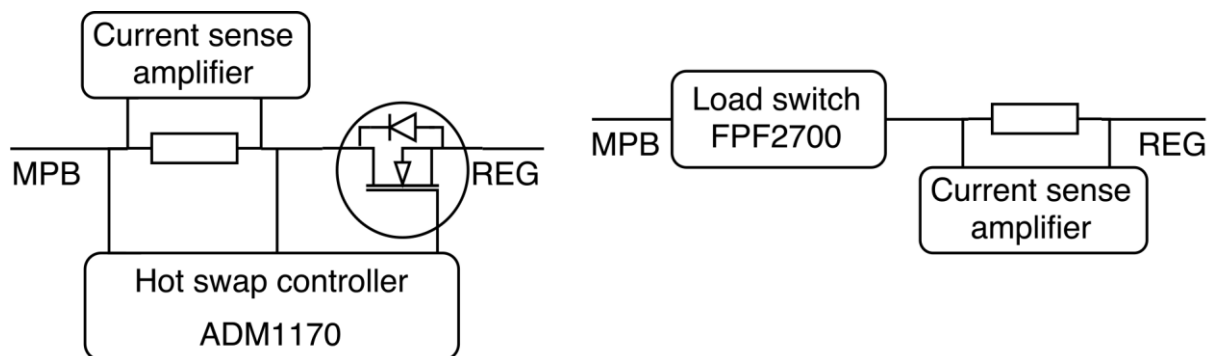


FIGURE 12. VOLTAGE CONVERSION INPUT STAGE PROPOSED SOLUTIONS

There are very few integrated load switches available for higher voltages than 5.5 V and even fewer for currents over 1 A. The FPF2700 is the only one (to the author's knowledge) that meets both of the requirements along with auto-reset functionality and a possibility to enable and disable the device. This device has also a major advantage as it has been tested for TID tolerance up to 24 krad [38].

The hot-swap controller basics are covered in chapter 5.5 and will not be repeated here. While there are many single channel hot-swap controllers available to choose from, the ADM1170

offered the best mix: small footprint, low quiescent current, good availability and no unneeded functionality or complexity. An alternative candidate could be the MAX5924 (Maxim Integrated), however this device was discovered after the ADM1170 had already been prototyped and there was no time to experiment with the device. The Maxim Integrated part has the advantage of a configurable circuit breaker limit using an external resistor, which means that a lower value shunt could be used. The features and parameters of both devices are compared in Table 5.

TABLE 5. COMPARISON BETWEEN THE TWO PROPOSED LOAD SWITCH DESIGNS

Feature	FPF2700	ADM1170
Maximum current	2 A	Not limited
Current limit accuracy	$\pm 20\%$	$\pm 12\%$
Resistance of the switch	88 m Ω (typical) 140 m Ω (maximum)	Depends on the current limit and the selected MOSFET: 35 m Ω for proposed solution
Thermal shutdown	YES	NO
Components required	1 IC, 3 passives	1 IC, 1 FET, 4 passives
External shunt	NO	YES
External power switch	NO	YES

Both devices were prototyped and they performed as expected based on information available in the datasheet. In order to measure the instantaneous current, an additional shunt has to be added into the system. For example, LT6102 CSA with a 20 m Ω shunt resistor could be used. This means that the total resistance of the FPF2700 based system would increase to 108–160 m Ω . ADM1170, however, already uses an external low value resistor to set the circuit breaker limit and the same shunt could be reused for sensing the instantaneous current, thus not adding any additional resistance. The ADM1170 based solution would have 3–5 times less resistance involved than the FPF2700 based solution, resulting in lower losses and higher efficiency.

It is very difficult to choose between the two solutions as one offers much higher efficiency, while the other one has known radiation behaviour. Emphasising reliability, it is the author's recommendation that the FPF2700 should be preferred until radiation testing data becomes available for the other device.

6.3. METHOD FOR VOLTAGE CONVERSION

The system needs to down-convert voltage from a floating bus varying between 6.6 to 8.4 V to a regulated bus of 3.3 V. Generally, there are three types of solutions for lowering voltage: a linear dropout regulator (LDO), a buck charge pump and an inductive buck DC/DC converter. The linear dropout regulator dissipates the leftover power $((V_{IN}-V_{OUT})\cdot I)$ into heat – meaning that the efficiency of the conversion drops as the voltage difference increases. Although the LDO is a very simple and robust component with high reliability, it would be far too inefficient for our application and managing the heat dissipation at higher loads would be challenging. The charge pump solution can be ruled out almost immediately because it does not allow for sufficient currents. The inductive buck DC/DC converter is much more complicated in nature than the previous two, but it is also capable of providing large currents at very high efficiencies.

The basic inductive switch-mode step-down converter consists of a switch, a diode, an inductor and an output capacitor. The basic principle of the converter is that it stores energy in the inductor when the switch is closed and then releases it into the load when the switch is open. The switch is driven with a pulse-width modulated (PWM) square wave of a varying duty cycle (under certain conditions, the frequency can vary also). The output capacitor helps to reduce the output voltage ripple and the diode completes the circuit when the switch is open. Figure 13 shows the connections between the aforementioned components.

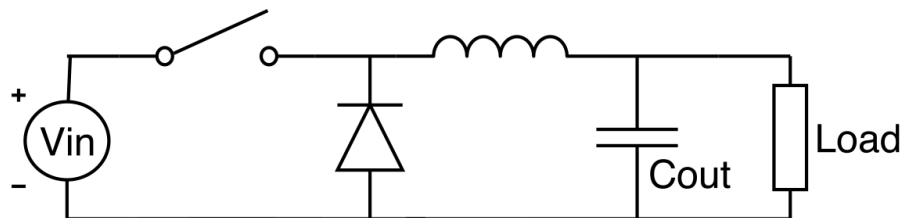


FIGURE 13. DC/DC STEP-DOWN CONVERTER BASIC CONSTRUCTION. V_{IN} DENOTES THE INPUT VOLTAGE SOURCE AND C_{OUT} DENOTES THE OUTPUT CAPACITOR

The converter generally has two operating modes: continuous and discontinuous. The continuous mode means that the inductor current does not drop to zero during the OFF period of the switch – this mode occurs when the output currents are larger. During the continuous mode, the output voltage is a function of the input voltage and the duty cycle. Should the output DC current become lower than the inductor ripple current (this typically happens during light loads), the converter starts operating in a discontinuous mode. In this mode, the inductor current reaches zero during the OFF period of the switch and it becomes much harder to control the

output voltage. The output voltage becomes a function of the input voltage, the output current, the inductance, the duty cycle and the switching frequency. [39]

In order to operate with various input and output voltages and supply different load currents stably and efficiently, the converter must operate in a closed loop. This requires feedback, which is most commonly taken from either the output voltage, the peak switch/inductor current or the output voltage ripple (hysteretic control). Each solution has its own pros and cons, which are covered in Table 6 [40] [41]. A further detailed description regarding the different feedback systems is beyond the scope of this work.

TABLE 6. OVERVIEW OF THE PROS AND CONS OF DIFFERENT DC/DC FEEDBACK SYSTEMS

Feedback mode	Pros	Cons
Output voltage	<ul style="list-style-type: none"> • Single simple control loop • Short ON-time possible • High noise tolerance 	<ul style="list-style-type: none"> • Slow response to fast changes to the input voltage (without line feedforward) • Complicated compensation
Inductor current	<ul style="list-style-type: none"> • Good response to input voltage changes • Simpler compensation • Highly stable feedback loop • Fast transient response • Low quiescent current 	<ul style="list-style-type: none"> • Complicated control due to two feedback loops • Minimum ON-time limited • Sensitive to poor layout
Output ripple	<ul style="list-style-type: none"> • Extremely fast transient response time • No compensation needed • Extremely simple and stable feedback loop 	<ul style="list-style-type: none"> • Difficult to achieve constant operating frequency • Hard to predict EMI • Large output ripple • Large output jitter • Use on low ESR ceramic capacitors complicated

6.4. CONVERTER EVALUATION AND SELECTION

The converters listed in Table 7 were chosen as candidates for the final system. The higher output current regulators (LT8614, LTC3603 and TPS51117) were chosen prior to the integrated bus concept, but were tested anyway because they had already been prototyped during the development of the testing platform by Mr. Raudheiding [32]. All converters exceed the required 6.6 to 8.4 V input voltage range with margin and de-rating included.

TABLE 7. CONVERTER CANDIDATE OVERVIEW

Parameter	LTC3601	LTC3603	LTC3624	LT8614	TPS51117	TPS62110
Mode	Current	Current	Current	Current	Hysteretic	Voltage
Rated I_{OUT}	1.5 A	2.5 A	2 A	4 A	Ext. limit ²	1.5 A
Max V_{OUT}	$V_{in} - 0.1$ V	$V_{in} - 0.5$ V	V_{in}	$V_{in} - 0.5$ V	5.5 V	$V_{in} - 1$ V
Operating frequency	820 kHz	720 kHz	1 MHz	480 kHz	250 kHz	1 MHz
Adjustable frequency	Yes	Yes	No	Yes	Yes	No
Package	QFN-16	QFN-20	MSOP-20	QFN-20	QFN-14	QFN-16
External components ³	5–8	8	1	6–7	10	2

During the testing campaign, the converters were tested at the output voltage of 3.3 V. They are also capable of providing 5 V, but if the de-rating suggestion is considered, TPS51117 fails to meet the requirement. Since the 5 V testing was not required by the bus at the time of writing the thesis, it is not included. Should the 5 V rail be required in the future, some components would have to be replaced on the prototype boards. As the testing routine and the analysis process is automated, it would only take a few hours to get the efficiency, ripple and voltage stability results.

One of the main considerations during the selection was the efficient operation in the discontinuous mode (light-load efficiency). As the expected dynamic operating range of the converter varies from tens of milliamps to 1.3 A, it is difficult to achieve high efficiency over the whole range. The converters from Linear Technology (LT and LTC prefix) have a special

² Uses external MOSFETs for switching

³ Feedback resistors (2), inductor and input/output capacitors not included

operating mode called burst mode in order to boost the efficiency during light-load operation. As the switching frequency and the duty cycle of the converter are quite low in the discontinuous mode, the device switches off all of the non-essential internal circuitry between the ON periods of the switch. This allows to reduce the quiescent current and increase efficiency. TPS62110 has a very similar approach to increasing efficiency. TPS

The second selection criteria was synchronous operation. This means that instead of a MOSFET and a diode, two MOSFETs are used. This reduces the losses during the OFF period and increases the efficiency. When comparing synchronous and non-synchronous rectification, it is true that synchronous operating mode is not always more efficient. This statement can be true during high duty cycle operation, but might not be true during lower duty cycle operation [42]. In continuous mode, the duty cycle is defined by the ratio of the input and output voltage and can be easily calculated. With a 3.3 V output and a 6.6 to 8.4 V input, the duty cycle would be 50–40%. As this is not very high, it seemed reasonable to use synchronous rectification. The special consideration involved with discontinuous operation and synchronous rectification is that the MOSFET is capable of bidirectional current flow. It has to be turned off when the current in the inductor reaches zero, otherwise the output capacitor would be drained through the inductor and the conversion efficiency would suffer greatly. This means that the converter must have additional circuitry to detect this event and take appropriate action in time. All the selected devices include this functionality.

A very important parameter of the DC/DC converters is their operating frequency. Higher switching frequencies can improve upon the output performance in terms of ripple voltage and transient response and it also allows for smaller inductive and capacitive components. On the other hand, the efficiency suffers with increasing frequencies due to switching losses [43]. As the application under consideration has a strong emphasis on efficiency, it was decided to rather use lower frequencies and larger components than to compromise on efficiency. For this reason a 1 MHz limit was imposed upon the maximum frequency. The lower frequency switching can mitigate potential electromagnetic emissions (EMI) problems. For adjustable frequency converters, the operating frequency was chosen based on the frequency-efficiency curve found in the datasheet.

Another very important criterion for the selection was that the converter had to be in a thermally enhanced package, meaning it must have a separate soldering pad underneath. This requirement

was set in order to reduce the probability of overheating, as the only viable way to transfer heat in space is by conduction.

During candidate selection, all major manufacturers were considered. Apparently, there were not many converters that fulfil all of the aforementioned requirements. Out of those that remained, some were discarded due to availability issues, others due to lack of in-depth documentation. Finally, only converters from Linear Technology and Texas Instruments remained. As the engineering team has had good experience with converters from those manufacturers on ESTCube-1, it seemed a sensible choice. Furthermore, a NASA compiled study of the most used CubeSat components show that Linear Technology and Texas Instruments power converters are the most used amounting to a total of 69% of the converters [44].

Low profile (< 3 mm) inductors were used in all the implementations with very similar DC resistance parameters. All chosen inductors have metal powder cores, which unfortunately are inferior to the ferrite based cores, but no suitable low profile ferrite core based inductors were available at the time of the selection. The 3 mm requirement originates from the system level bus design limitation. Should this requirement change, the inductor selection will be revisited.

All converters used the same amount of input and output capacitance: 30 μF of multilayer ceramic capacitors (MLCC) for the input and 100 μF tantalum along with 20 μF of MLCC for the output. Ceramic capacitors were in the standard 1210 (imperial) package with nominal capacitance of 10 μF .

All designed modules have components on both sides as this enables to minimize the footprint of the converter and reduce the area of the high current loops. All specific design recommendations given by the datasheets were respected when possible.

In the following sections, mainly the results for 8.4 and 7.4 V input voltages are covered, as the main operating voltage will vary between those voltages. This is due to intentionally limiting the depth of discharge of the batteries. Measurement results not covered in the following chapters can be found in the appendix.

6.4.1. VOLTAGE CONVERSION EFFICIENCY

The conversion efficiency is one of the most important parameters of a voltage converter. As the energy production on-board the satellite is limited, converters with the highest efficiency are obviously preferred. The results in Figure 14 show the calculated efficiency curves over the

whole measured range. All converters were tested to the same output current regardless that some were more capable than others. The values in Figure 15 show how much more efficient the converters are at 7.4 V than at 8.4 V. Per regulator comparisons at all three different input voltages are available in the appendix.

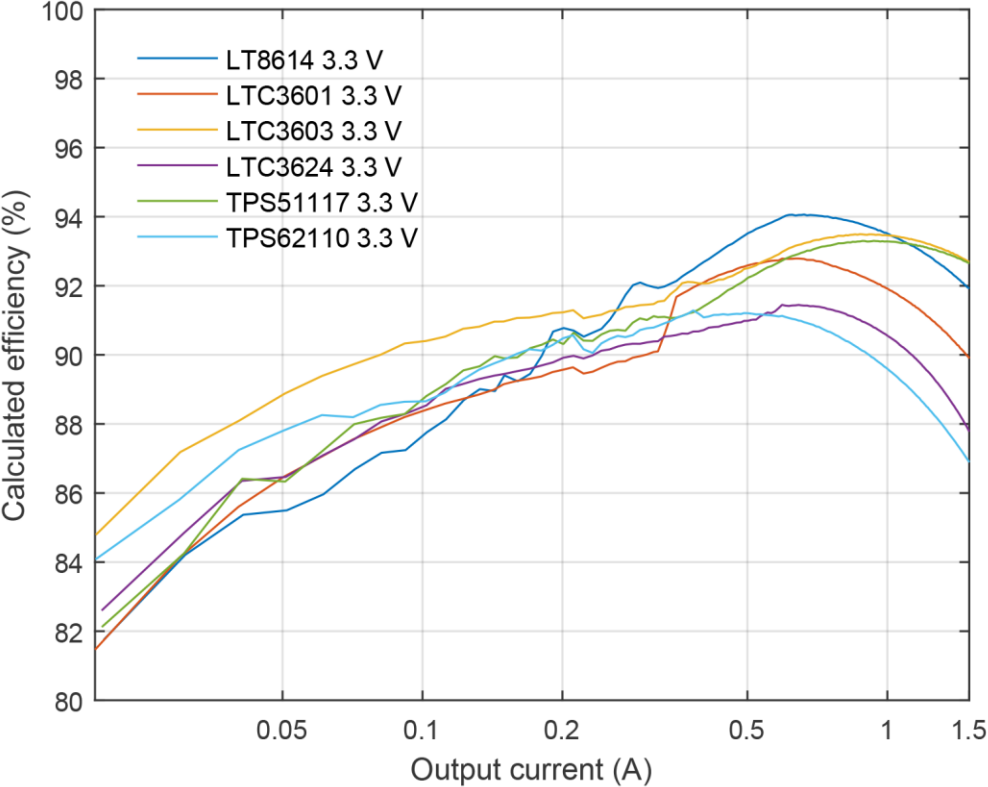


FIGURE 14. DC/DC CONVERTER EFFICIENCY AT 8.4 V INPUT AND 3.3 V OUTPUT VOLTAGE IN LOGARITHMIC SCALE EMPHASISING LIGHT-LOAD EFFICIENCY

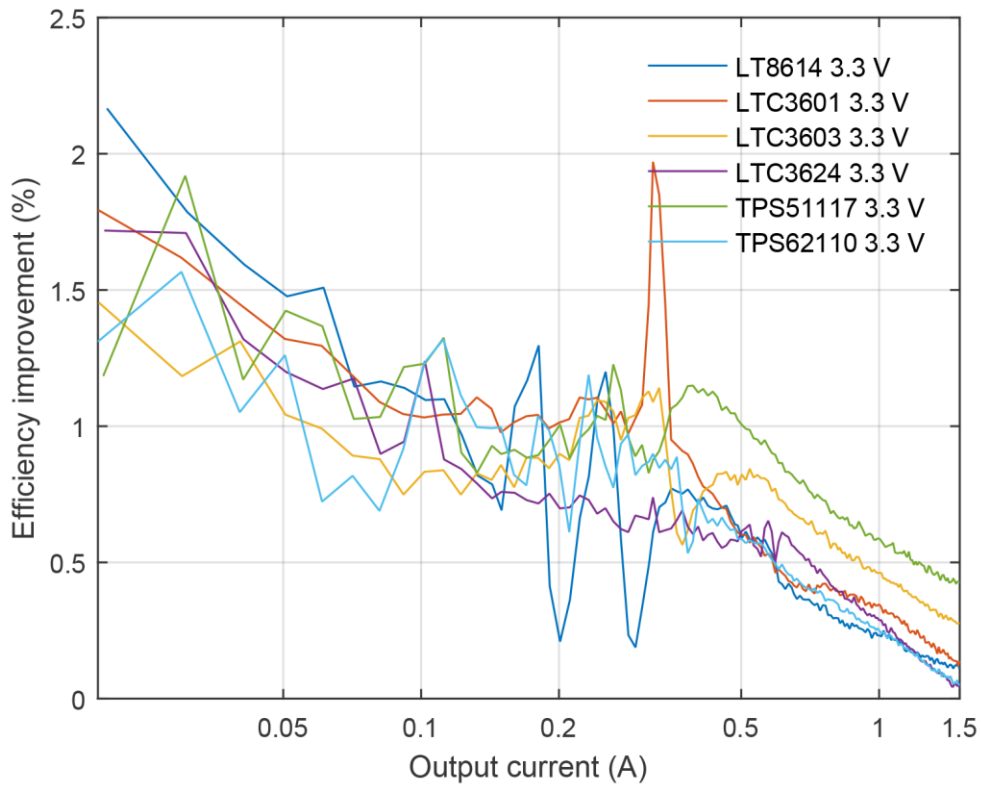


FIGURE 15. CHANGE IN EFFICIENCY WHEN INPUT VOLTAGE IS DECREASED FROM 8.4 V TO 7.4 V. LARGER VALUES INDICATE LARGER INCREASE IN EFFICIENCY

In general, most converters exhibit quite similar performance in terms of efficiency. It can also be seen that the efficiency increases quite similarly when the voltage is lowered from 8.4 V to 7.4 V. Based on the efficiency results, the best candidate seems to be LTC3603 as it offers the highest performance over the whole range. Closely following are LT8614 and TPS51117. If the decision was to be made purely on efficiency, it would be very difficult.

6.4.2. VOLTAGE STABILITY

The output voltage stability of the converters was tested by measuring and logging output voltage at the converter feedback point over the full current range. Voltage dependency of the converter input voltage was also investigated. None of the converters showed any considerable input voltage dependencies. The largest changes in the output voltage were less than 10 mV and those were exhibited by the only voltage-mode regulator TPS62110. The changes for the other converters were within the margin of error. Figure 16 shows how the output voltages are affected by the output current.

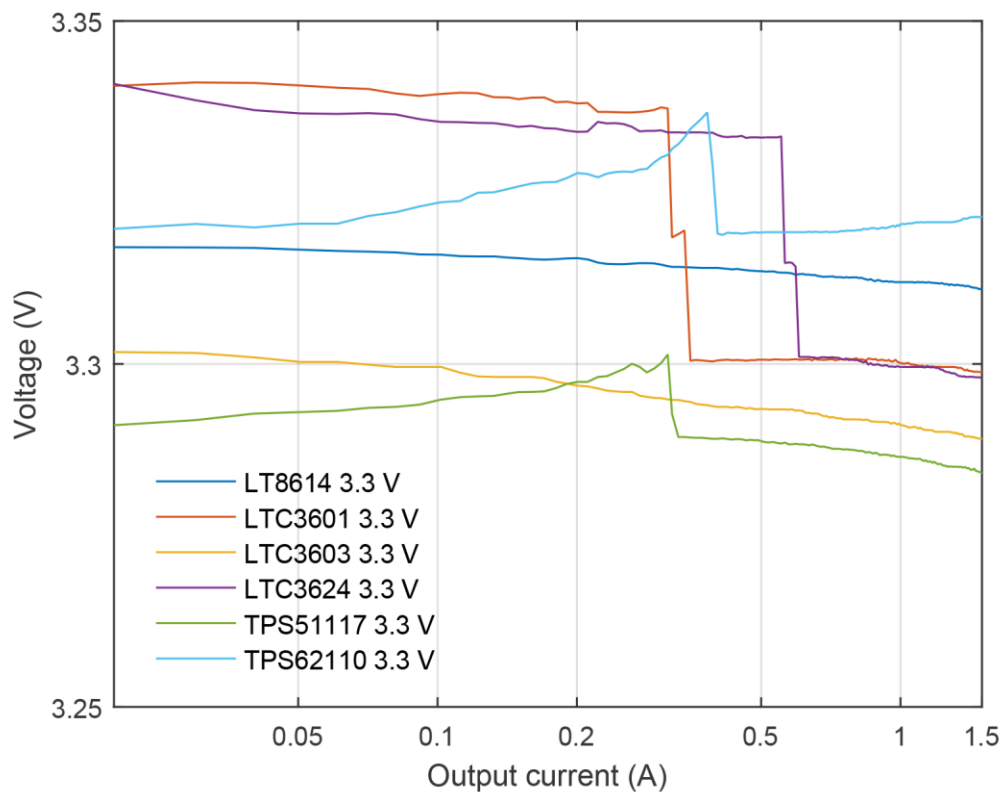


FIGURE 16. DC/DC VOLTAGE STABILITY AT 8.4 V INPUT AND 3.3 V OUTPUT VOLTAGE

The steps seen in the figure are most likely caused by the transition from the discontinuous to the continuous mode. The absolute accuracy of the output voltage is not as important as only 1% accurate resistors were used for the prototype and there are bound to be small voltage drops beyond the feedback measurement location. The most important conclusion is that the converters can keep the output stable regardless of the current being sourced.

6.4.3. OUTPUT VOLTAGE RIPPLE

As there was no strict requirement set for the output voltage ripple, it would have been possible to skip the measurement. However, this parameter was measured to see whether there are any serious issues with the output ripple. The nature of the ripple generally shows if the converter output has enough bypass capacitance present with the right equivalent series resistance (ESR) present [45]. The results also provide the other subsystems with an indication of what quality power supply should be expected and how much power supply filtering would be required on their end.

The input voltage independence was investigated first. For most converters the results showed that the output ripple does not depend on the input voltage. The only noticeable difference was

with the TPS51117 at 6.6 V input voltage. The differences were in the order of 10 mV peak-to-peak when compared to the results at higher input voltages. As the converter would be operating at that low voltage only in case of emergency, it was not considered a major issue. Due to the ripple results being effectively independent of the input voltage and consistent in shape, they were averaged.

Next, the results from two different modules were compared. As both modules were tested in both measurement channels, a total of four sets of results were measured. The channel-wise (same module tested in both channels) results overlapped very nicely and there was no considerable difference. However, some modules performed slightly differently – this might be due to output capacitor quality, converter internals or some other component tolerances.

Table 8 summarises the worst case performance. The crossover between the discontinuous and continuous operating modes can be seen quite clearly from the plots as the ripple performance changes significantly. Plots of the results are available in the appendix.

TABLE 8. WORST CASE RIPPLE PERFORMANCE OF THE TESTED CONVERTER MODULES

Converter	Discontinuous operation		Continuous operation		Crossover current (mA)
	Max ripple (mV)		Max ripple (mV)		
	V _{PP}	V _{RMS}	V _{PP}	V _{RMS}	
LT8614	11	3	11	3	200
LTC3601	33	8	16	5	500
LTC3603	40	15	10	3	500/750 ⁴
LTC3624	52	17	8	2	750
TPS51117	30	10	29	6	300
TPS62110	34	10	4	1	500

Based on discontinuous mode results, the top three converters are LT8614, TPS51117 and LTC3601; based on continuous mode: TPS62110, LT3603 and LT8614. All around, LT8614 seems to be the best performing converter ripple wise. It also has the lowest threshold for crossing over to continuous operation, which results in stable switching frequency at lower output currents. TPS51117 has much higher ripple in the continuous mode compared to other

⁴ Modules changed operating modes at different frequencies

converters because it operates based on hysteretic control loop – it uses output ripple as the feedback for the internal control loop.

6.4.4. TRANSIENT RESPONSE

Transient response testing can reveal issues in the feedback loop compensation of a voltage converter. If the feedback loop is under-compensated, the output of the converter tends to oscillate after a transient event. If the loop is over-compensated, it takes a long time to return to the nominal output voltage. It is acceptable, if a suddenly changing load causes a small overshoot or undershoot in the output voltage, should it smoothly recover from it. [34]

The converters were subjected to two different tests: increase from zero load to maximum load of 1.45 A and increase from 80 mA to 1.45 A. The first test was meant to simulate the worst case condition that the converter could theoretically be exposed to. The second test was conducted with the purpose of investigating transition between discontinuous mode and continuous mode. Voltage over- and undershoots (V_{OS} and V_{US}) were recorded along with the time that it took for the converter to recover (t_{REC}).

TABLE 9. TRANSIENT RESPONSE MEASUREMENT RESULTS

Converter	0 A → 1.45 A		1.45 A → 0 A		80 mA → 1.45 A		1.45 A → 80 mA	
	V_{US}	t_{REC}	V_{OS}	t_{REC}	V_{US}	t_{REC}	V_{OS}	t_{REC}
LT8614	150	60	100	10000	150	60	100	400
LTC3601	80	25	120	10	- ⁵		110	3
LTC3603	50	30	100	6000	50	25	100	75
LTC3624	260	100	150	5000	200	100	150	75
TPS51117	25	30	200	5000	25	3	100	50
TPS62110	75	50	150	100	100	50	110	100

The testing did not uncover any serious stability issues with the converters as no ringing was observed. Top three converters in terms of response time are: LTC3601, TPS51117 and LTC3603. If we look at the voltage deviations from the nominal value, LTC3603, TPS51117 and LTC3601 have the top performance.

⁵ No distinguishable transient response was observed. Increased ripple of 50 mV peak-peak was observed for 60 μ s, after that the ripple returned to 30 mV peak-peak.

6.4.5. NEAR-FIELD ELECTROMAGNETIC EMISSIONS

Radiated electromagnetic emissions in the near-field were also measured as part of the testing campaign. The aim of these measurements was to get an idea how the converters emissions differ and which circuit elements emit the most noise. This information might give critical insight later on when planning the system and component level placements inside the integrated bus as the components are packed tightly together. The emissions were measured at 8.4 V input voltage and three different output currents: 0.1 A, 0.5 A and 1.5 A.

Largest amount of emissions were given off by the switching elements of the converter, which makes sense because the largest current fluctuations happen there. It has to be noted that the inductors gave off much weaker emissions than the switching elements, due to being magnetically shielded. If similar routing topology is used for the final system (controller on one side of the board and inductor directly underneath it), the controller should be on the side that is away from the more sensitive parts. If possible, sensitive circuits should be located on a different board and ideally in another section of the bus. This definitely applies to the communications system. It was also interesting to see how much magnetic energy was radiated at the planned communication frequencies. The full measurement results can be seen in appendix.

Based on the measurements around the 430 MHz band (estimated communication frequency), top three converters are TPS51117, LTC3603 and LT8614. If the full range is considered, the LT8614 outperforms all others, but this is not a surprise as it is advertised as a low EMI converter.

6.4.6. CONVERTER TESTING CONCLUSION

Based on the testing results discussed earlier, it is the author's recommendation to use LTC3603 converter for the final solution. This seems a reasonable choice as the converter has performed very well in all of the conducted tests. It can also provide more current than is required (up to 2.5 A) by the present system. This means that the converter, even at the maximum load, will run under lower stress and, should some larger changes be made to the system that increase the current consumption significantly, it could still be used as is.

Should higher level testing reveal that LTC3603 could not be used for some reason, LT8614 could be considered as an alternative as it also shows very good performance, especially electromagnetic emissions and output ripple wise.

6.5. CONVERTER OUTPUT OR CONNECTION AND LOAD SHARING

In order to make the system redundant, there have to be two stand-alone converters. With this requirement, there is the issue of connecting their outputs to the regulated voltage bus. On ESTCube-1 this was done through low-dropout Schottky diodes. The solution worked, however, it also had a large impact on the system's overall efficiency due to the power dissipated in the Schottky diodes.

To improve this system and minimize unnecessary losses, a system based on a specialized load-sharing ideal diode controller (LTC4370 from Linear Technology) was built and tested. This device can work either in a load-sharing mode, in which it distributes the load evenly between two converters, or in a more simplified dual ideal diode mode, where it just prevents reverse currents. Low-dropout Schottky diodes (DB2430700L from Panasonic) have been implemented in parallel with the driven MOSFETs. These are for the sake of redundancy, should the control electronics malfunction. Figure 17 illustrates the developed system and Figure 18 compares the losses in the Schottky diode operating mode and the ideal diode operating mode.

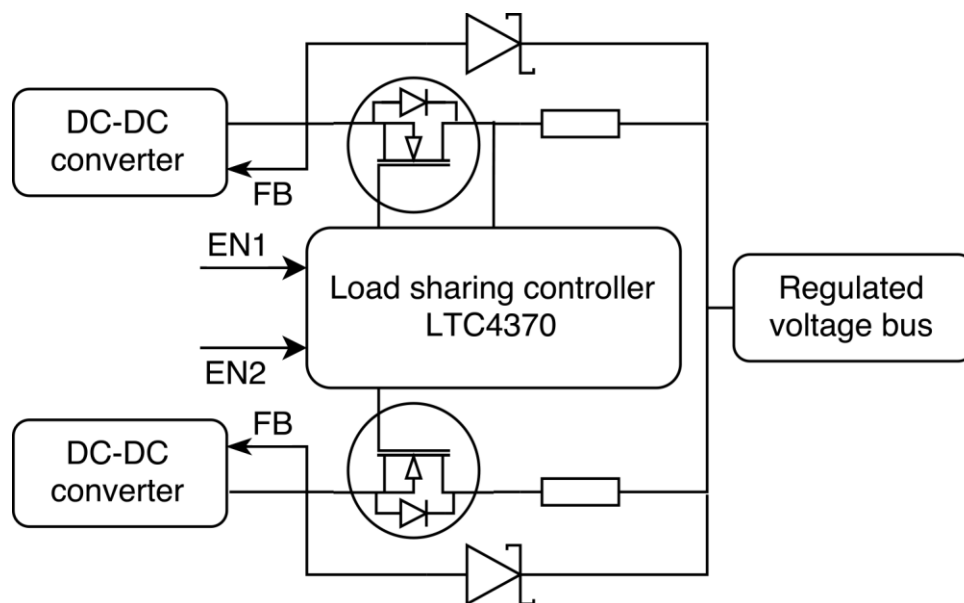


FIGURE 17. VOLTAGE CONVERSION OUTPUT STAGE

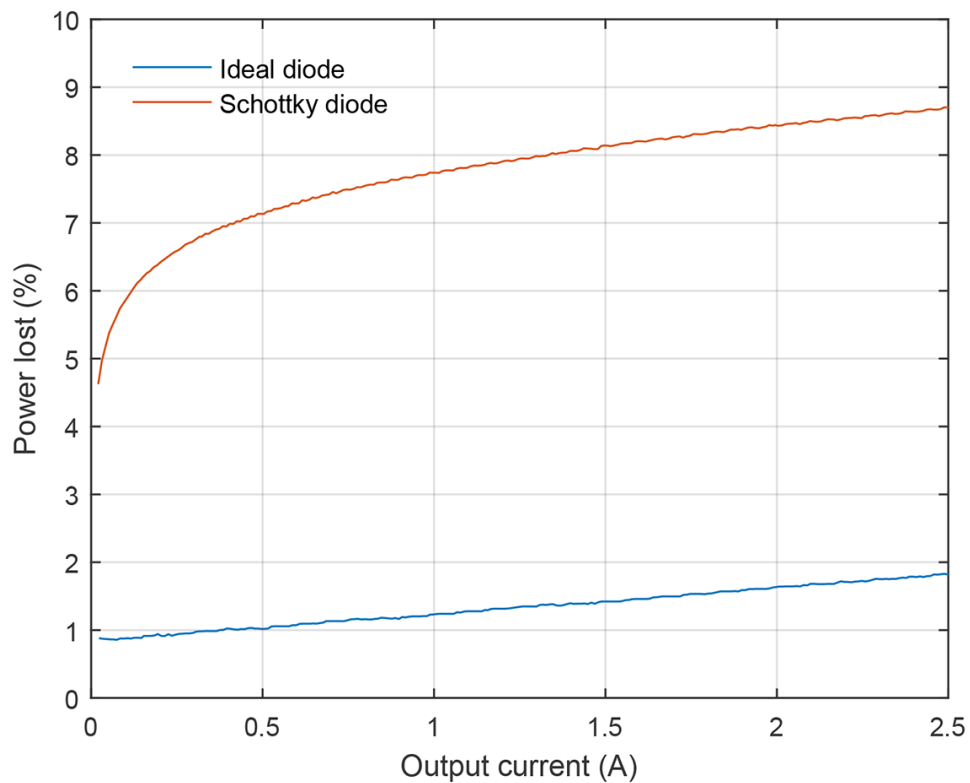


FIGURE 18. CALCULATED LOSSES COMPARISON BETWEEN SCHOTTKY AND IDEAL DIODE BASED CIRCUITS (BASED ON MEASUREMENT DATA)

The previous EPS design envisioned that regulated voltages would be distributed to all of the systems at much higher currents. With the load sharing functionality it would have been possible to subject the converters to lower loads and even increase upon efficiency under certain conditions. The current plan for the EPS foresees that the device would rather operate in the basic dual ideal-diode mode and lower the ORing losses substantially. As the load-sharing requirement is not present any more, it might be reasonable to swap the dual channel controller for two simpler single channel controllers. As this is a quite recent idea, it is not covered in this thesis.

6.6. POWER DISTRIBUTION CIRCUITRY

The power distribution circuitry has the task of protecting the consumers from excessive current draw and the (un)regulated voltage rails from short circuits caused by the consumers. The point is to isolate the faulty system from the others, so it would not affect the power availability for the rest of the satellite. The EPS will distribute power to system level consumers (other subsystems and payloads) within the satellite – the component level power distribution will be handled by the consumers themselves. As covered earlier, the regulated voltage rail will be

distributed only within the integrated bus, while the unregulated battery bus will be also shared with the payloads. As there are two different voltage rails that will be distributed (fixed 3.3 V and floating 6.6–8.4 V), they can be viewed separately.

For the 3.3 V rail it is possible to use lower voltage load switches, such as TPS2553 (Texas Instruments) and TPS2557 (Texas Instruments). The former is an improved version of the TPS2551 (Texas Instruments) which was successfully used on-board ESTCube-1. The latter has direct flight heritage from ESTCube-1 where it was operated 24/7 in the battery protection circuit [18]. These devices should easily fulfil the needs of the systems on the 3.3 V rail. External current sensing is required in addition to the load switch and depending on the accuracy required, can be implemented with either LTC6102 or LTC6105 (flight heritage from ESTCube-1).

The power distribution for the battery bus will use the same solutions discussed in the chapter 6.2. FPF2700 could be used for the systems with lower current requirements. Beyond 1.5 A, the ADM1170 based solution should be used to minimize the losses and voltage drop. The previously mentioned current sensing approach would also be adequate for this system.

7. SUMMARY

In this thesis, the design for the electrical power system of the ESTCube-2 nanosatellite was proposed. The effort was mainly focused on the development of the battery management and protection system, along with the voltage conversion and power distribution system. Special hardware and software solutions that enabled repeatable and rapid testing were developed by the author or under the supervision of the author.

Most important results of this thesis are:

- A flight-proven EPS architecture was adapted for the new integrated bus based system
- A set of requirements was compiled for the battery management and protection system, and the voltage conversion and power distribution system
- Out of the two battery management schemes considered, the LTC4226 based system was recommended for the final implementation
- For the voltage conversion and power distribution system, multiple load switch designs were evaluated and recommendations were made when and where to use which devices
- Out of six voltage converters originally considered, LTC3603 was chosen due to its high efficiency, excellent transient response, low output ripple and low EMI emissions in the frequency region of interest

Although two major sections of the EPS were investigated in this work, the system is still far from complete. In the next phase of development, the systems discussed in this work will have to be integrated onto a single circuit board along with the microcontroller and its peripherals. This platform would be a prerequisite for software development and the integration testing campaign involving other systems. Additionally, the energy harvesting system, which was not covered in this thesis, is still awaiting testing and may need additional development before it could be tested with the previously mentioned systems.

Süsteemi arhitektuur ning komponentide valimine ESTCube-2 toitealamsüsteemi jaoks

Erik Ilbis

8. KOKKUVÕTE

Käesolevas töös esitati süsteemikavand ESTCube-2 nanosatellidi toitealamsüsteemi jaoks. Töö põhiohk on suunatud akuhaldussüsteemi ning pingemuundamis- ja energiajaotussüsteemi uurimisele, kavandamisele ning testimisele. Töös kasutatud spetsiaalsed riistvara- ning tarkvaralahendused töötati välja autori poolt või autori juhendamisel.

Töö kõige olulisemad tulemused on:

- kosmoses töötamise pärandiga toitealamsüsteemi arhitektuur kohandati edukalt uue integreeritud baassüsteemi jaoks;
- koostati nõuete kogum akuhaldussüsteemi ning pingemuundamis- ja energiajaotussüsteemi jaoks;
- kahest kaalutud variandist valiti välja LTC4226-1 baseeruv akuhaldussüsteem, kuna sellel on vastuvõetavad kaod ning väga madal valmisolekuvool;
- energiajaotussüsteemi jaoks kaaluti mitut erinevat võimsuslülituse lahendust ning leiti sobilikud lahendused erinevate kasutusolukordade jaoks;
- kuuest testitud pingemuundurist soovitab autor kasutada pingemuundurit LTC3603, kuna kõnealusel seadmél on kõrge efektiivsus, madal väljundpinge säbarlainetus ning see kiirgab vähe elektromagnetilist energiat huvipakkuvas sagedusvahemikus.

Hoolimata sellest, et selle töö raames uuriti kahte põhilist toitealamsüsteemi osa, on süsteem veel kaugel lõplikust kujust. Järgmises arenduse faasis tuleb käesolevad süsteemid integreerida ühele trükkplaadile koos mikrokontrolleril baseeruva juhtimissüsteemiga. Eelmainitud süsteem on eelduseks edasisele tööle, mis hõlmab endas nii tarkvaraarendust kui ka integratsiooniteste teiste alamsüsteemidega. Lisaks on veel vaja testida energiakogumiseks mõeldud süsteemi, mis võib vajada täiendavaid muudatusi enne, kui seda saab katsetada koos ülejäänud süsteemiga.

ACKNOWLEDGEMENTS

I would like to thank my supervisors Mihkel Pajusalu and Artur Abels for their support and advice given throughout the course of this work. Without their advice and guidance, this work would have not been possible. Many thanks to Martin Põder and Karl-Indrek Raudheiding, for their contributions to the EPS development.

I would also like to thank Mart Noorma for starting the ESTCube programme and granting us such amazing opportunities and Andris Slavinskis for leading the programme for the past few years. Additionally, I would like to thank Viljo Allik, Henri Kuuste and Lauri Mihkels for their consultations and advice. And of course, rest of the ESTCube team for their contribution.

Finally, I would like to thank my parents for their support and my girlfriend for putting up with the long working hours (again), which seem to disappear into the satellite development.

REFERENCES

- [1] California State Polytechnic University, “CubeSat Design Specification revision 13,” 2014.
- [2] M. Swartwout, “CubeSat Database,” [Online]. Available: <https://sites.google.com/a/slu.edu/swartwout/home/cubesat-database>. [Accessed 13 May 2016].
- [3] W. Ley, K. Wittmann and W. Hallmann, Handbook of Space Technology, John Wiley & Sons, 2009.
- [4] S. Lätt, A. Slavinskis, E. Ilbis, U. Kvell, K. Voormansik, E. Kulu, M. Pajusalu, H. Kuuste, I. Sünter, T. Eenmäe, K. Laizans and e. al, “ESTCube-1 nanosatellite for electric solar wind sail in-orbit technology,” *Proceedings of the Estonian Academy of Sciences*, vol. 63, no. 2S, p. 200–209, 2014.
- [5] P. Janhunen, P. K. Toivanen, J. Polkko, S. Merikallio, P. Salminen, E. Haeggström, H. Seppänen, R. Kurppa, J. Ukkonen, S. Kiprich, G. Thornell, H. Kratz, L. Richter, O. Krömer, R. Rosta, M. Noorma, J. Envall, S. Lätt, G. Mengali, A. A. Quarta and H. Koivisto, “Invited Article: Electric solar wind sail: Toward test missions,” *Review of Scientific Instruments*, no. 81, 2010.
- [6] J. Envall, P. Janhunen, P. Toivanen, M. Pajusalu, E. Ilbis, J. Kalde, M. Averin, H. Kuuste, K. Laizans, V. Allik, T. Rauhala, H. Seppänen, S. Kiprich, J. Ukkonen, E. Haeggström, T. Kalvas, O. Tarvainen, J. Kauppinen, A. Nuottajärvi and H. Koivisto, “E-sail test payload of the ESTCube-1 nanosatellite,” *Proceedings of the Estonian Academy of Sciences*, vol. 63, no. 2S, pp. 210-221, 2014.
- [7] H. Ehrpais, I. Sünter, E. Ilbis, J. Dalbins, I. Iakubivskyi, E. Kulu, I. Ploom, P. Janhunen, J. Kuusk, J. Šate, R. Trops and A. Slavinskis, “ESTCube-2 Mission and Satellite Design,” in *The 4S Symposium*, Valletta, 2016.
- [8] P. Janhunen, “Coulomb drag devices: electric solar wind sail propulsion and ionospheric deorbiting,” in *Space Propulsion*, Köln, 2014.

- [9] J. Šate, R. Trops, E. Briede, A. Orbidāns, M. Donerblics and R. Pabērzs, “Concept of the spectrally efficient CubeSat communication subsystem,” *Space review*, vol. 4, 2016.
- [10] E. Ilbis, “ESTCube-1 Electrical Power System – Design, Implementation and Testing,” Tartu, 2013.
- [11] R. Rice, “Design of a High Power Cube Satellite Power System,” in *28th Annual AIAA/USU Conference on Small Satellites*, Logan, 2014.
- [12] EPS Team of PW-Sat2, “PW-Sat2 Electrical Power System Preliminary Design Review,” Warsaw, 2015.
- [13] A. I. L. Telgie, J. Bouwmeester and F. Stelwagen, “FLIGHT Results and Lessons Learnt from the Delfi-n3XT Electrical Power Subsystem Operations,” in *65th International Astronautical Congress*, Toronto, 2014.
- [14] A. Shrivastav, S. Singh, A. Mahajan and S. Bhattacharya, “Effective control & software techniques for high efficiency GaN FET based flexible electrical power system for cube-satellites,” in *IEEE Applied Power Electronics Conference and Exposition (APEC)*, Long Beach, 2016.
- [15] J. Hemmo, “Electrical Power Systems for Finnish Nanosatellites,” Espoo, 2013.
- [16] B. Lynch and C. Wallace, “CubeSat electronic power system,” Santa Clara, 2013.
- [17] A. I. L. Telgie, “Design and analysis of the DelFFi solar energy supply,” Delft, 2014.
- [18] M. Pajusalu, E. Ilbis, T. Ilves, M. Veske, J. Kalde, H. Lillmaa, R. Rantus, M. Pelakauskas, A. Leitu, K. Voormansik, V. Allik, S. Lätt, J. Envall and M. Noorma, “Design and Pre-Flight Testing of the Electrical Power System for the ESTCube-1 Nanosatellite,” *Proceedings of the Estonian Academy of Sciences*, vol. 63, no. 2S, pp. 232-241, 2014.
- [19] A. Slavinskis, M. Pajusalu, H. Kuuste, E. Ilbis, T. Eenmäe, I. Sünter, K. Laizans, H. Ehrpais, P. Liias, E. Kulu, J. Viru, J. Kalde, U. Kvell, J. Kütt, K. Zalite, K. Kahn, S. Lätt, J. Envall, P. Toivanen, J. Polkko, P. Janhunen, R. Rosta, T. Kalvas, R. Vendt, V. Allik and M. Noorma, “ESTCube-1 In-Orbit Experience and Lessons Learned,” *Aerospace and Electronic Systems Magazine*, vol. 30, no. 8, August 2015.

- [20] M. Pajusalu, E. Ilbis, T. Ilves, R. Raabe, M. Veske, G. Olentšenko, E. Briede, S. Lätt and M. Noorma, “Electrical Power System for ESTCube-1 Nanosatellite: Lessons Learned from In-Orbit Operations,” in *65th International Astronautical Congress*, Toronto, 2014.
- [21] T. Ilves, “ESTCube-1 Electrical Power System operation software,” Tartu, 2013.
- [22] R. Ghaffarian, “SMT Solder Joint Reliability/Workmanship Environmental Test Results Correlation for LCC Assemblies,” 1995.
- [23] NASA, “Workmanship Standard For Surface Mount Technology,” 1999.
- [24] I. Baylako and M. Hudaverdi, “Reliability Concerns of Radiation Effects on Space Electronics,” Ankara, 2007.
- [25] R. Maurer, M. Fraeman, M. Martin and D. Roth, “Harsh Environments: Space Radiation Environment, Effects, and Mitigation,” *Johns Hopkins APL Technical Digest*, vol. 28, no. 1, 2008.
- [26] P. Truscott, R. Nartallo, F. Lei, D. Heynderickx, S. Bourdarie and A. Sicard- Piet, “Integrated Radiation Mitigation and Shielding Design,” 2010.
- [27] A. C. Tribble, *The Space Environment Implications for Spacecraft Design*, Princeton: Princeton University Press, 2003.
- [28] “IEEE Standard for Environmental Specifications for Spaceborne Computer Modules,” IEEE, 1997.
- [29] NASA, “NASA/GSFC Radiation Effects & Analysis,” 26 April 2016. [Online]. Available: <http://radhome.gsfc.nasa.gov/top.htm>. [Accessed 26 April 2016].
- [30] ECSS Secretariat, “Space Product Assurance - Derating - EEE components,” ESA-ESTEC Requirements & Standards Division, Noordwijk, 2011.
- [31] M. Pöder, “Prototype Design of ESTCube-2 Electrical Power System Control Electronics,” Tartu, 2014.
- [32] K.-I. Raudheiding, “Testing of Voltage Converters for the Electrical Power System of ESTCube-2,” Tartu, 2015.

- [33] Artesyn, “Verification of Power Converter Performance,” Artesyn.
- [34] Texas Instruments, “AN-1733 Load Transient Testing Simplified,” Texas Instruments, 2007.
- [35] J. Polonský , “MightyWatt Arduino Electronic Load,” [Online]. Available: <http://kaktuscircuits.blogspot.com/2014/02/mightywatt-arduino-electronic-load.html>. [Accessed 11 May 2016].
- [36] Y. Barsukov and J. Qian, *Battery Power Management for Portable Devices*, Artech House, 2013.
- [37] D. Laude, “Ideal Diode Controller Eliminates Energy Wasting Diodes in Power OR-ing Applications,” *Linear Technology Journal*, vol. 12, no. 4, 2002.
- [38] R. Kingsbury, F. Schmidt, K. Cahoy and D. Sklair, “TID Tolerance of Popular CubeSat Components,” in *Nuclear and Space Radiation Effects Conference*, San Francisco, 2013.
- [39] Texas Instruments, “Understanding Buck Power Stages in Switchmode Power Supplies,” Texas Instruments, 1999.
- [40] S. Maniktala, “Voltage-Mode, Current-Mode (and Hysteretic Control),” Microsemi, 2012.
- [41] ROHM Semiconductor, “Control Methods (Voltage Mode, Current Mode, Hysteresis Control),” ROHM Semiconductor, 6 December 2015. [Online]. Available: <http://micro.rohm.com/en/techweb/knowledge/dcdc/s-dcdc/02-s-dcdc/97>. [Accessed 16 May 2016].
- [42] A. Fagnani, “Synchronous rectification boosts efficiency by reducing power loss,” *Analog Applications Journal*, vol. Q2 2013, pp. 9-12, 2013.
- [43] R. Nowakowski and B. King, “Choosing the optimum switching frequency of your DC/DC converter,” *EE Times*, 2006.
- [44] K. Beckwith and J. Skinner, “NASA Electronic Parts and Packaging (NEPP) Program: CubeSat Parts Lists and Supply Chain,” in *NASA Electronics Technology Workshop*, 2014.

[45] R. Sponar, R. Faltus, M. Jane, Z. Flegr and T. Zednicek, "DC/DC Converter Output Capacitor Benchmark," AVX, Lanskroun.

APPENDIX – ADDITIONAL MEASUREMENT RESULTS

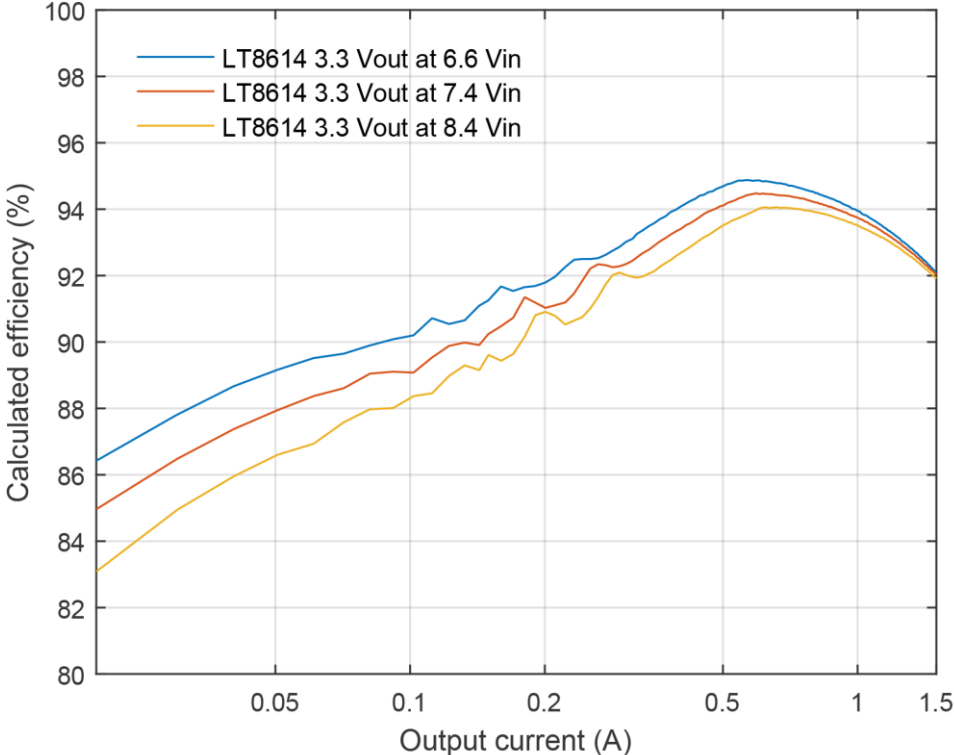


FIGURE 19. VOLTAGE CONVERSION EFFICIENCY FOR LT8614 AT THREE INPUT VOLTAGES

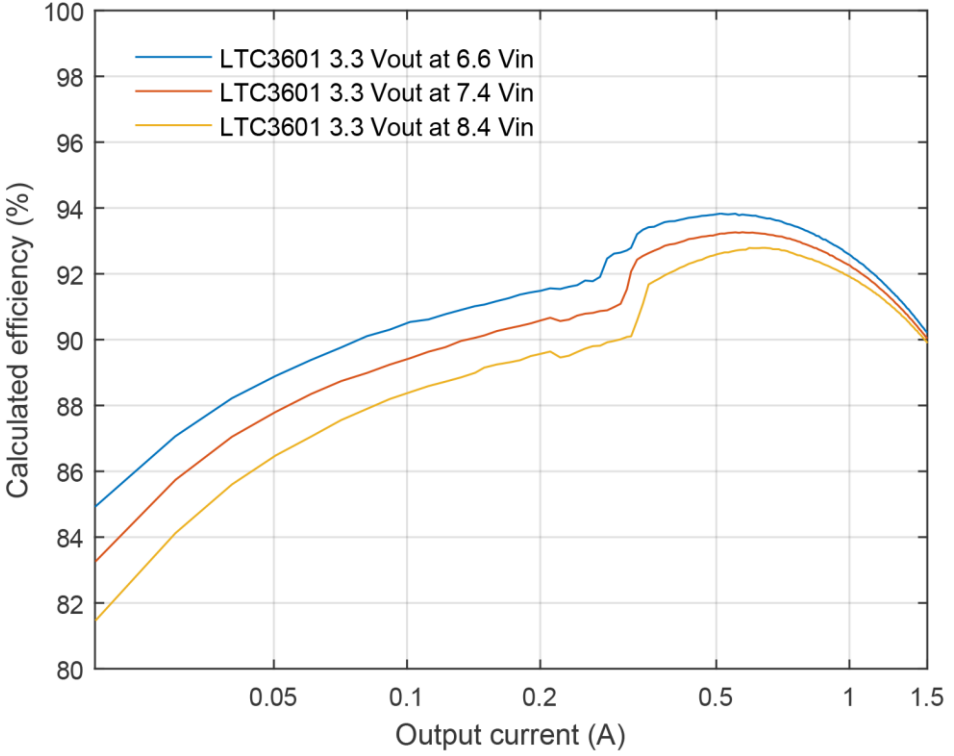


FIGURE 20. VOLTAGE CONVERSION EFFICIENCY FOR LTC3601 AT THREE INPUT VOLTAGES

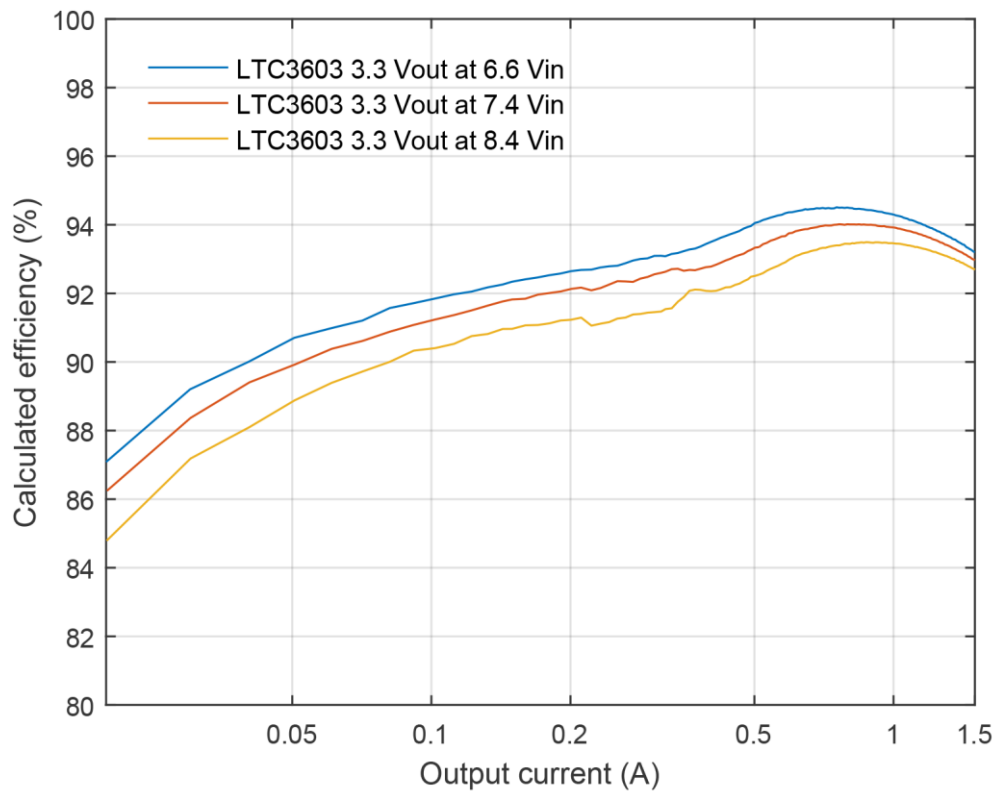


FIGURE 21. VOLTAGE CONVERSION EFFICIENCY FOR LTC3603 AT THREE INPUT VOLTAGES

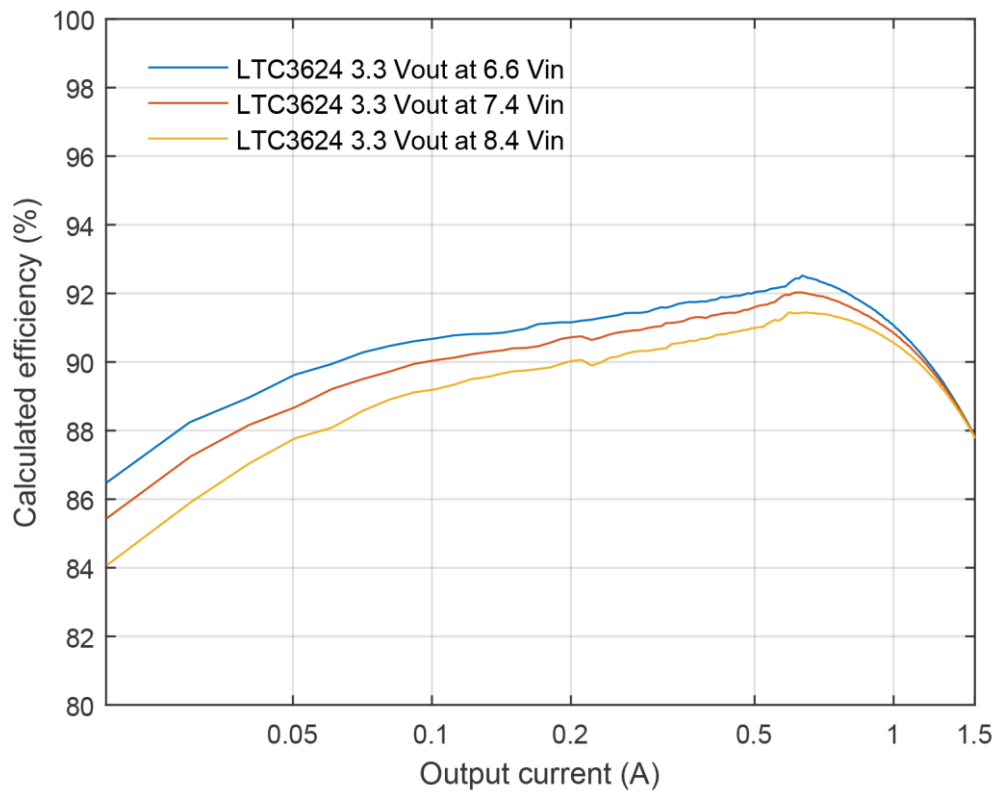


FIGURE 22. VOLTAGE CONVERSION EFFICIENCY FOR LTC3624 AT THREE INPUT VOLTAGES

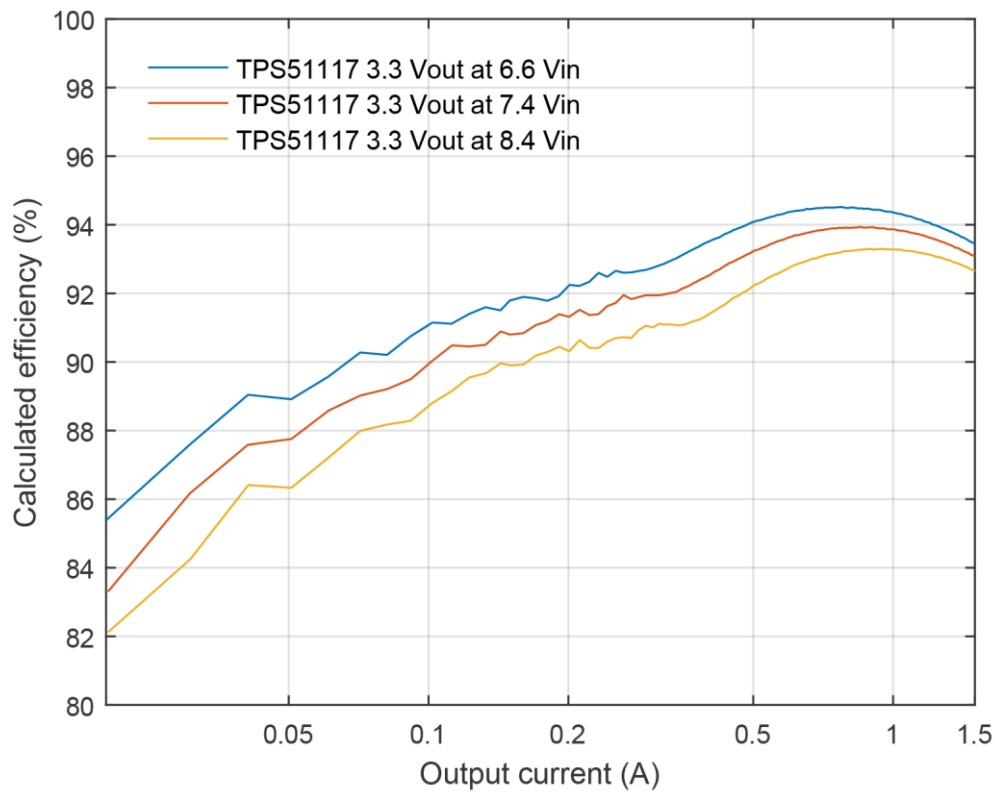


FIGURE 23. VOLTAGE CONVERSION EFFICIENCY FOR TPS51117 AT THREE INPUT VOLTAGES

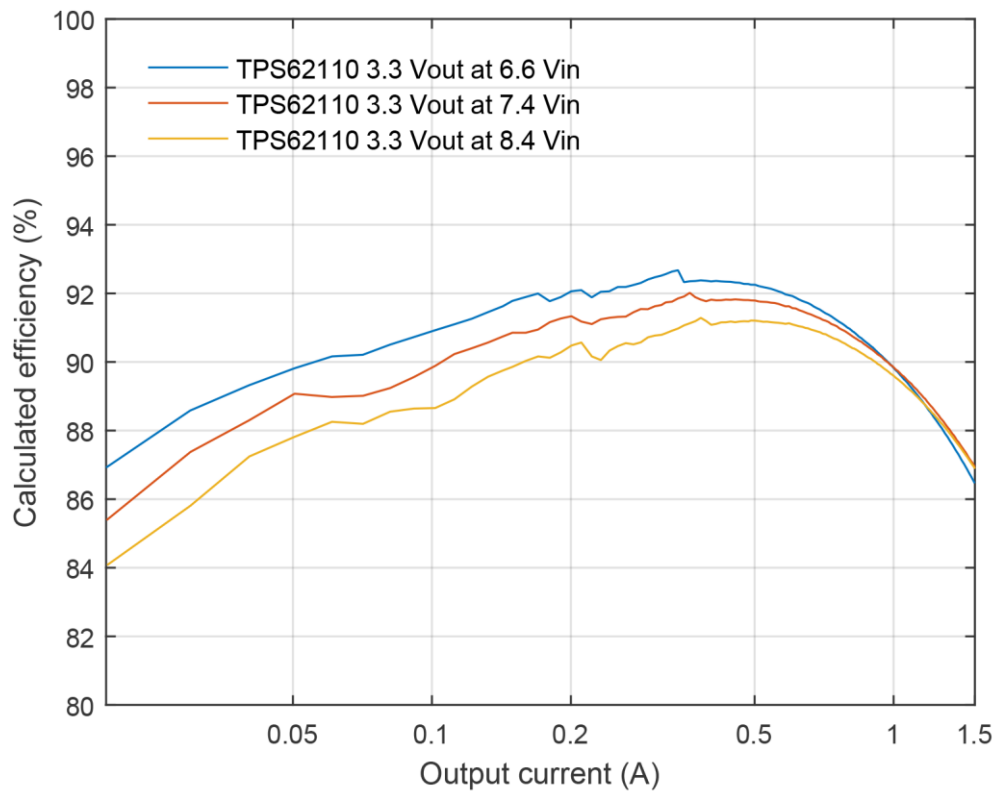


FIGURE 24. VOLTAGE CONVERSION EFFICIENCY FOR TPS62110 AT THREE INPUT VOLTAGES

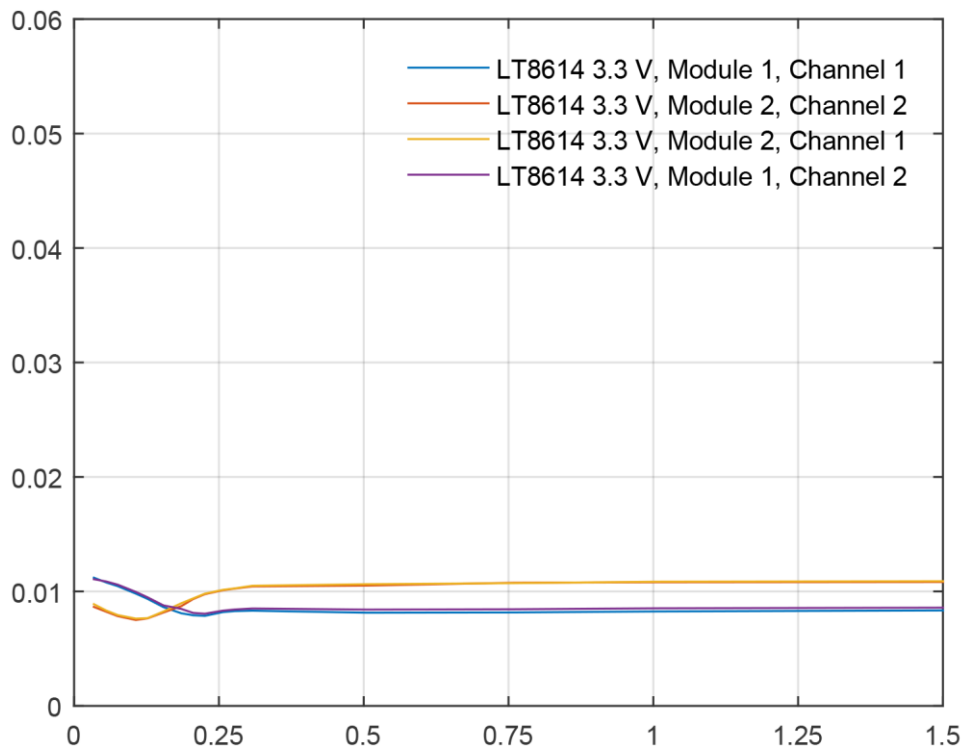


FIGURE 25. LT8614 PEAK-TO-PEAK RIPPLE MEASUREMENTS

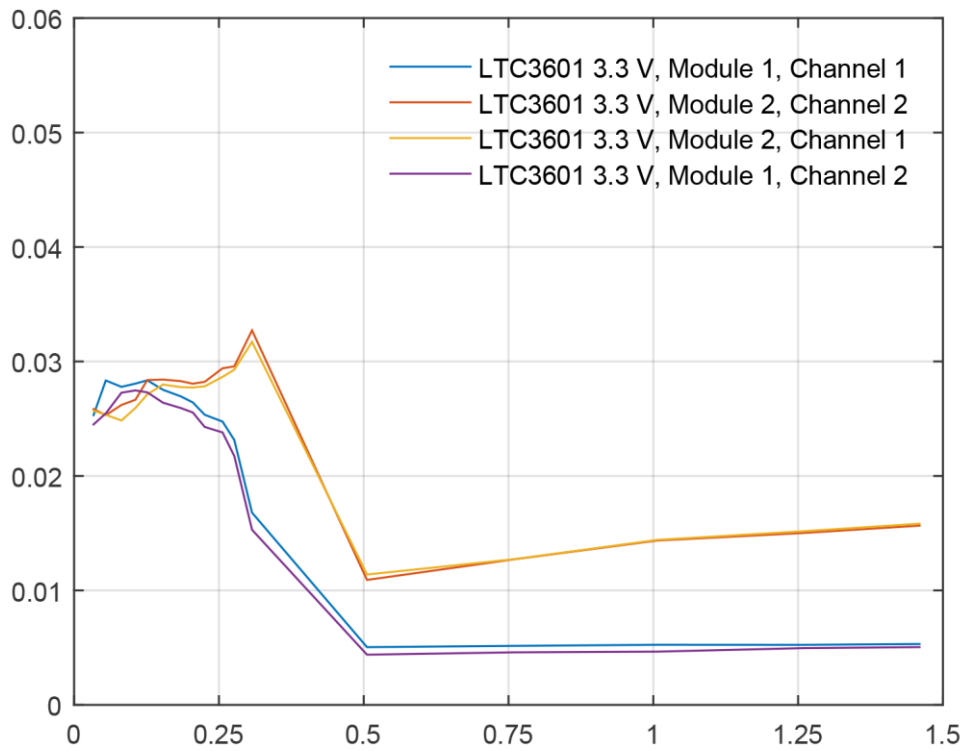


FIGURE 26. LTC3601 PEAK-TO-PEAK RIPPLE MEASUREMENTS

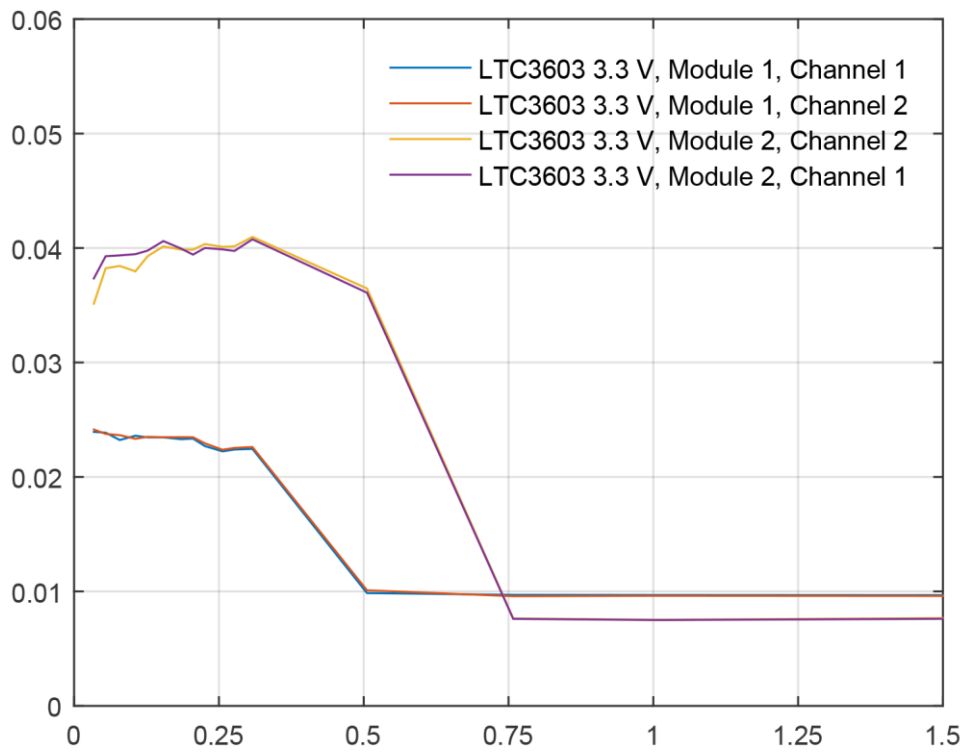


FIGURE 27. LTC3603 PEAK-TO-PEAK RIPPLE MEASUREMENTS

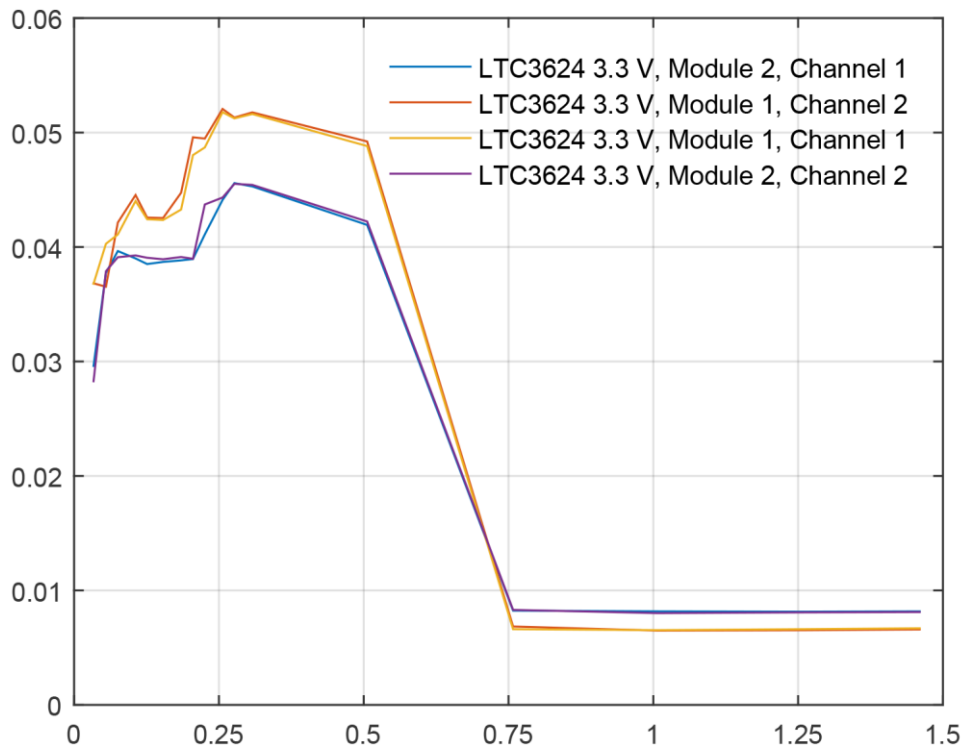


FIGURE 28. LTC3624 PEAK-TO-PEAK RIPPLE MEASUREMENTS

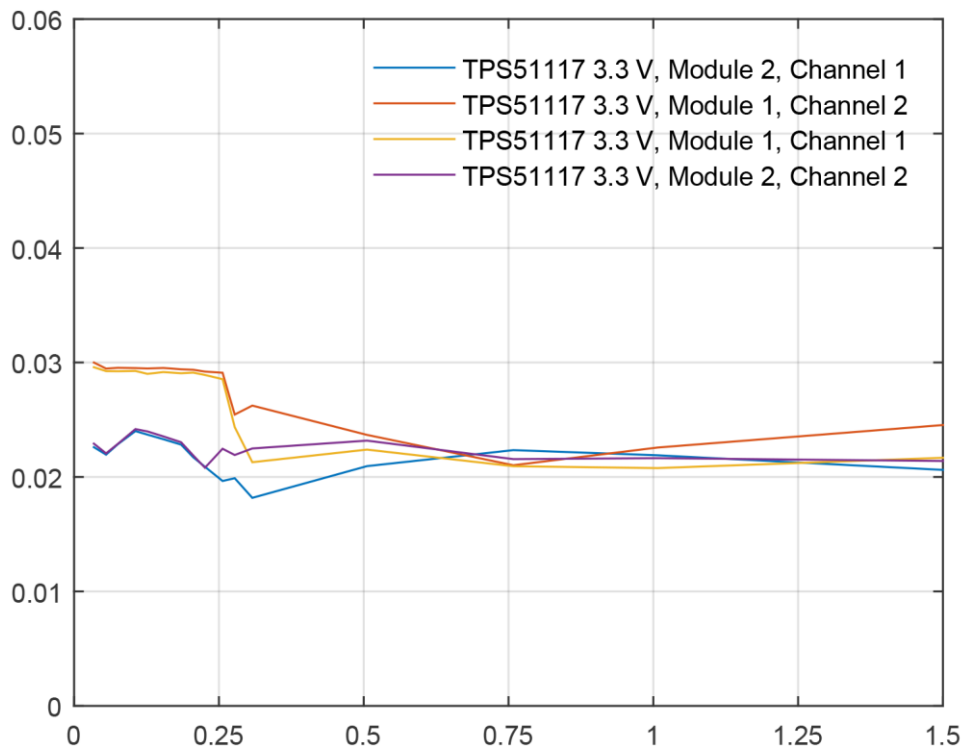


FIGURE 29. TPS51117 PEAK-TO-PEAK RIPPLE MEASUREMENTS

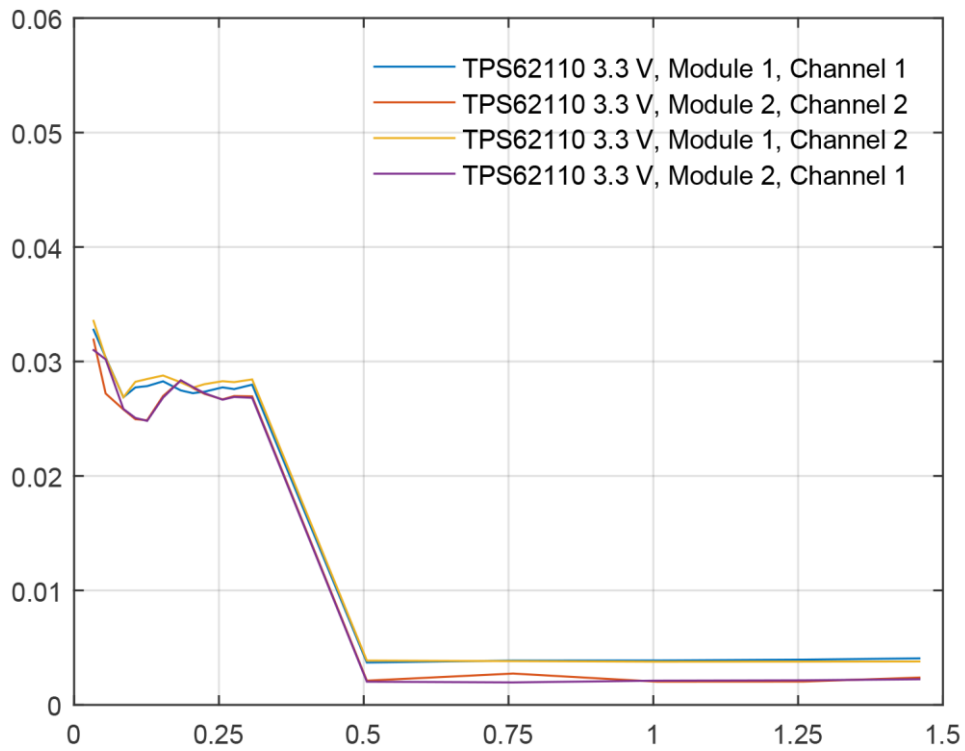


FIGURE 30. TPS62110 PEAK-TO-PEAK RIPPLE MEASUREMENTS

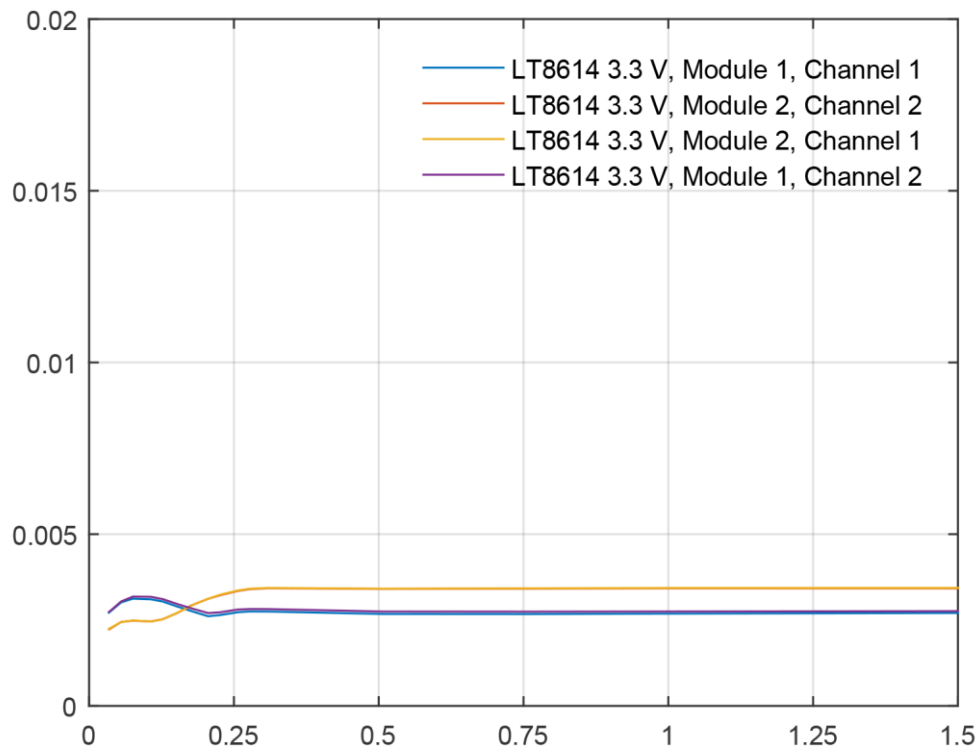


FIGURE 31. LT8614 RMS RIPPLE MEASUREMENTS

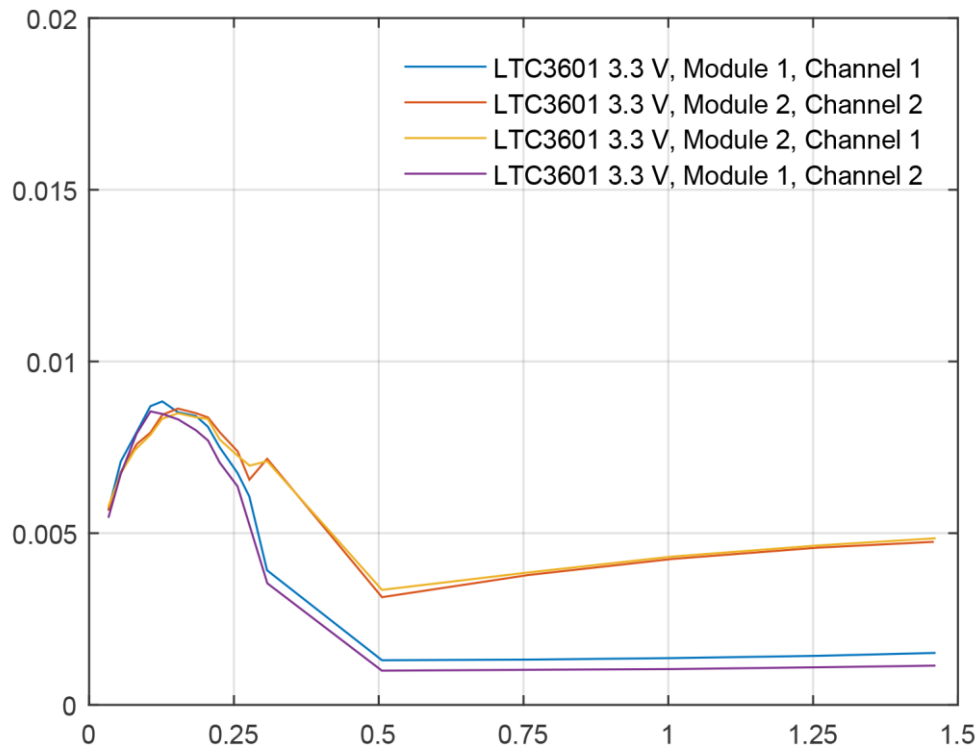


FIGURE 32. LTC3601 RMS RIPPLE MEASUREMENTS

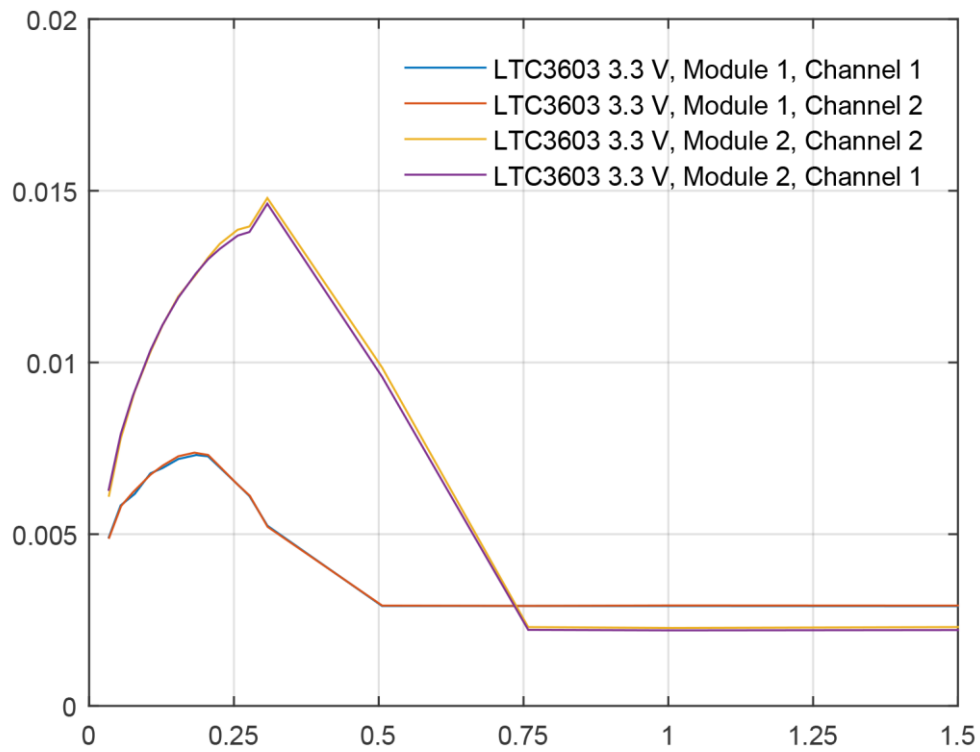


FIGURE 33. LTC3603 RMS RIPPLE MEASUREMENTS

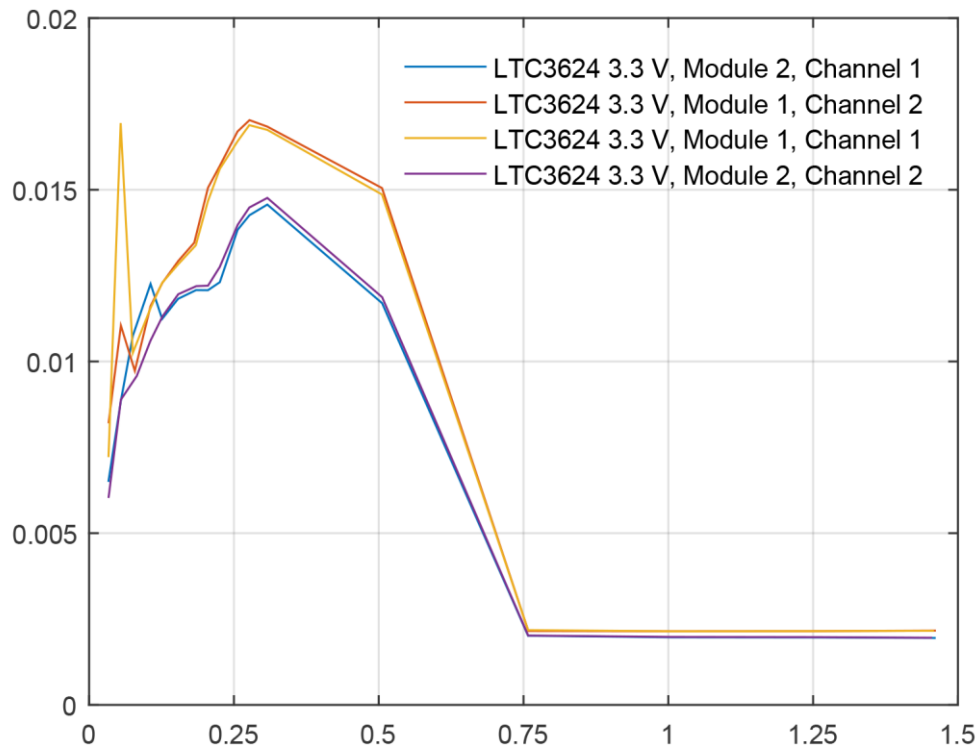


FIGURE 34. LTC3624 RMS RIPPLE MEASUREMENTS

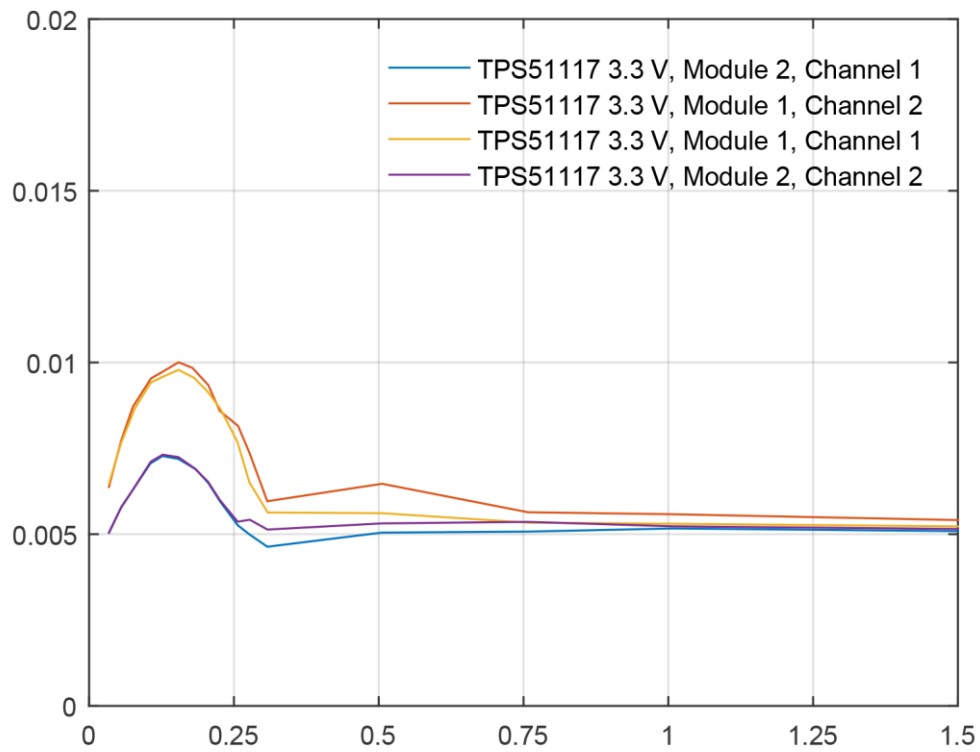


FIGURE 35. TPS51117 RMS RIPPLE MEASUREMENTS

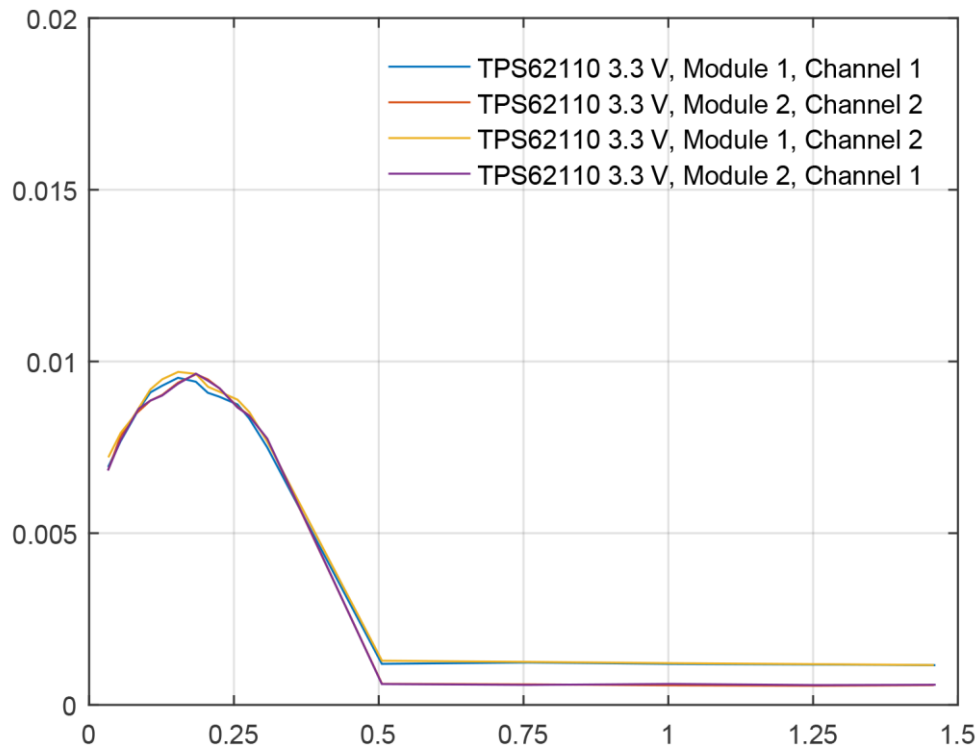


FIGURE 36. TPS62110 RMS RIPPLE MEASUREMENTS

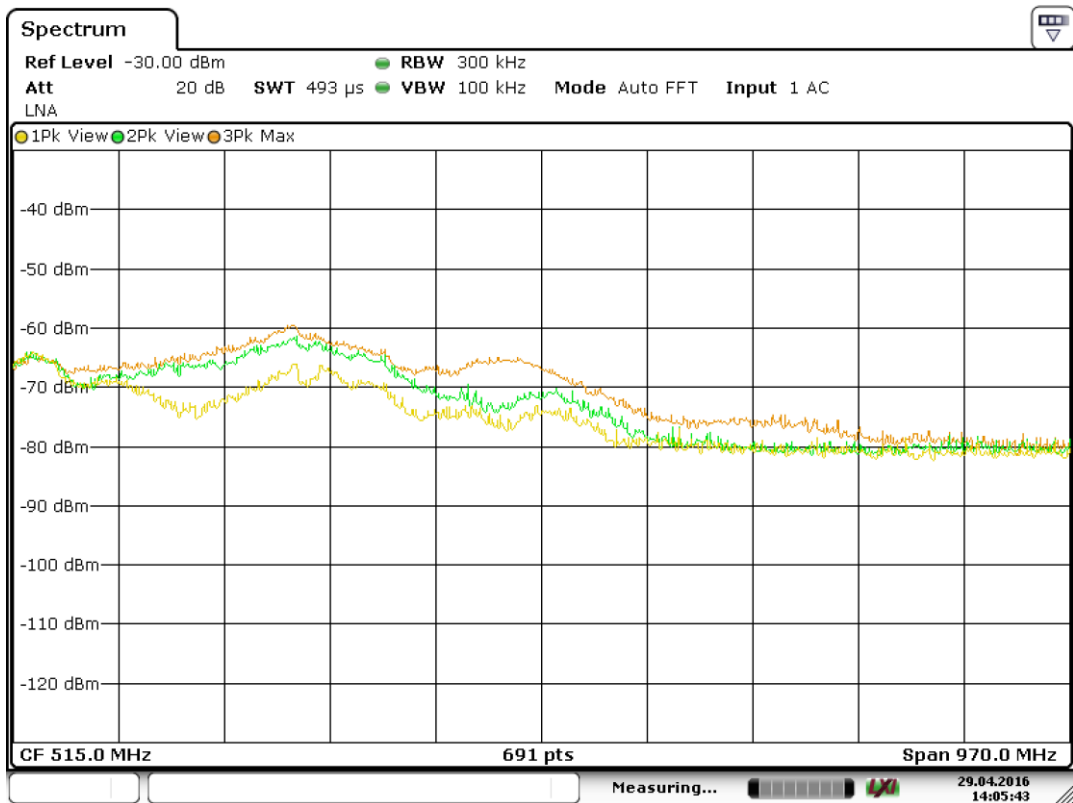


FIGURE 37. LT8614 NEAR-FIELD EMI RESULTS (YELLOW 0.1 A, GREEN 0.5 A, ORANGE 1.5 A)

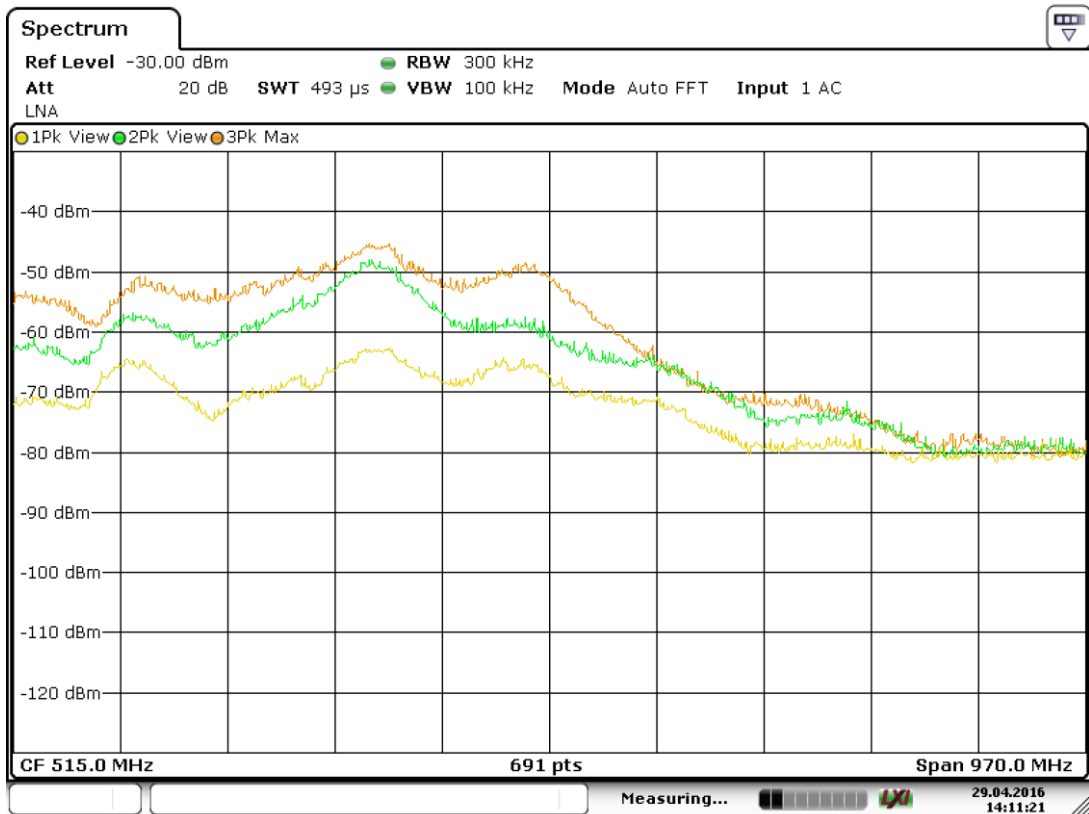


FIGURE 38. LTC3601 NEAR-FIELD EMI RESULTS (YELLOW 0.1 A, GREEN 0.5 A, ORANGE 1.5 A)

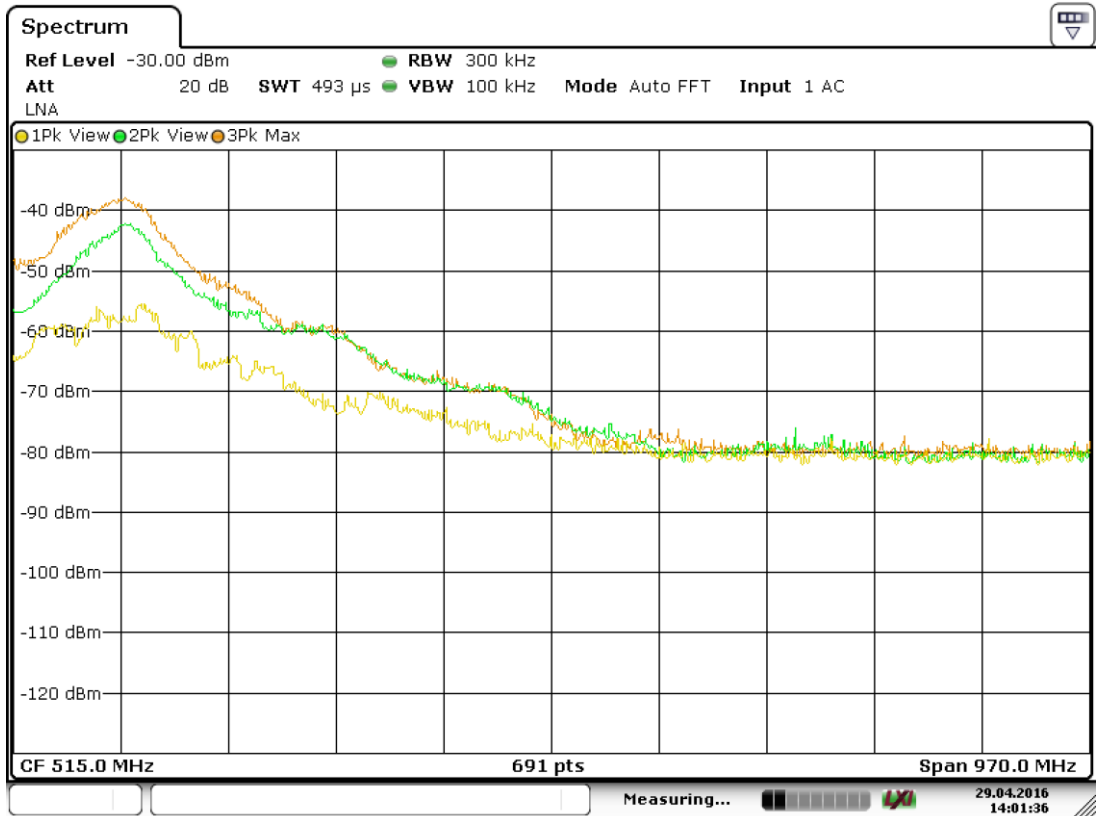


FIGURE 39. LTC3603 NEAR-FIELD EMI RESULTS (YELLOW 0.1 A, GREEN 0.5 A, ORANGE 1.5 A)

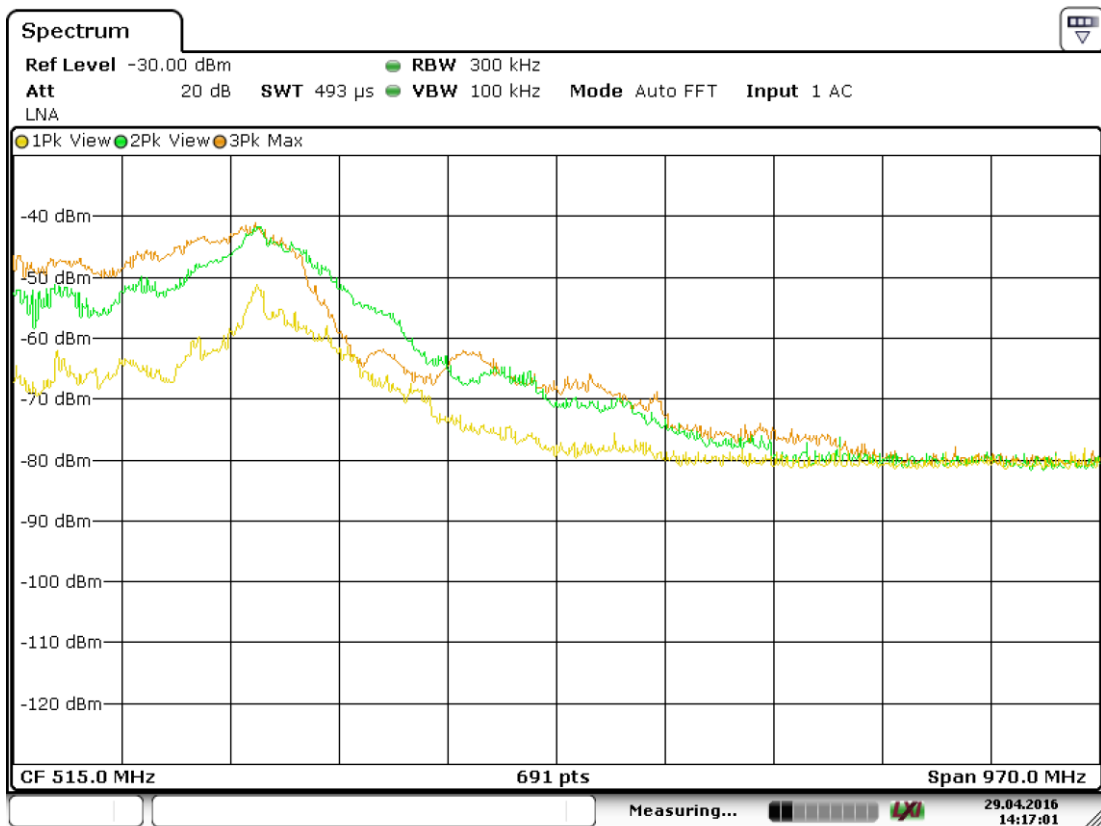


FIGURE 40. LTC3624 NEAR-FIELD EMI RESULTS (YELLOW 0.1 A, GREEN 0.5 A, ORANGE 1.5 A)

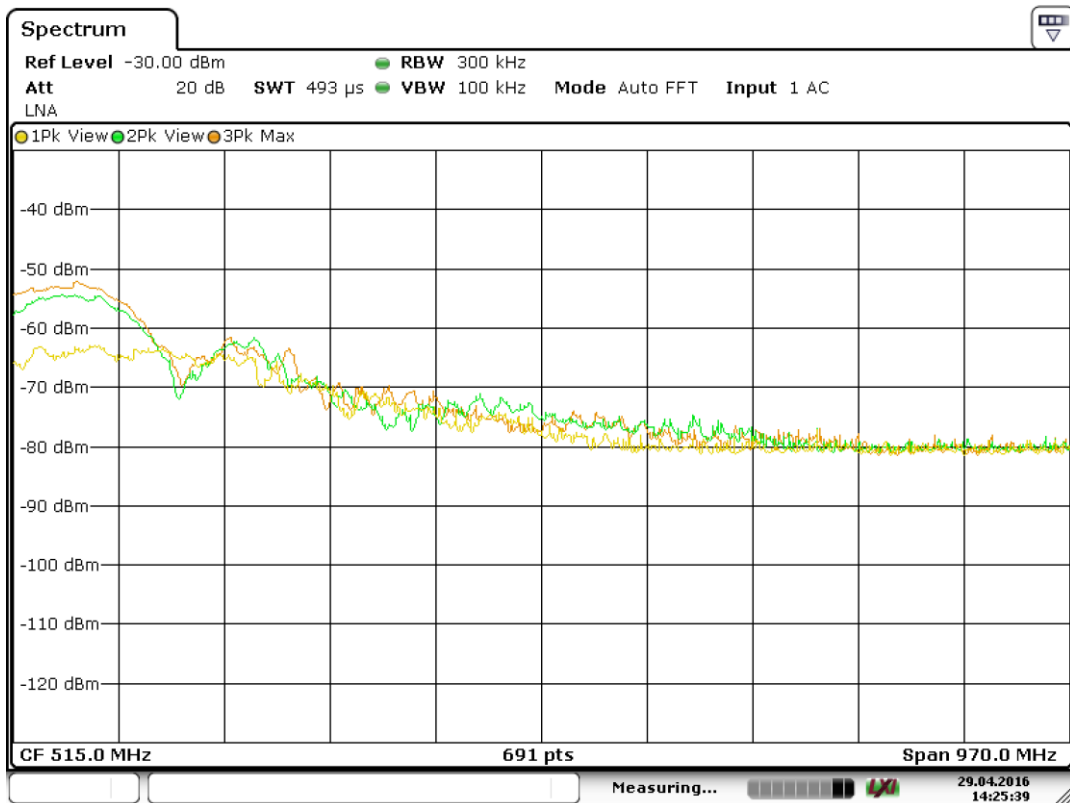


FIGURE 41. TPS51117 NEAR-FIELD EMI RESULTS (YELLOW 0.1 A, GREEN 0.5 A, ORANGE 1.5 A)

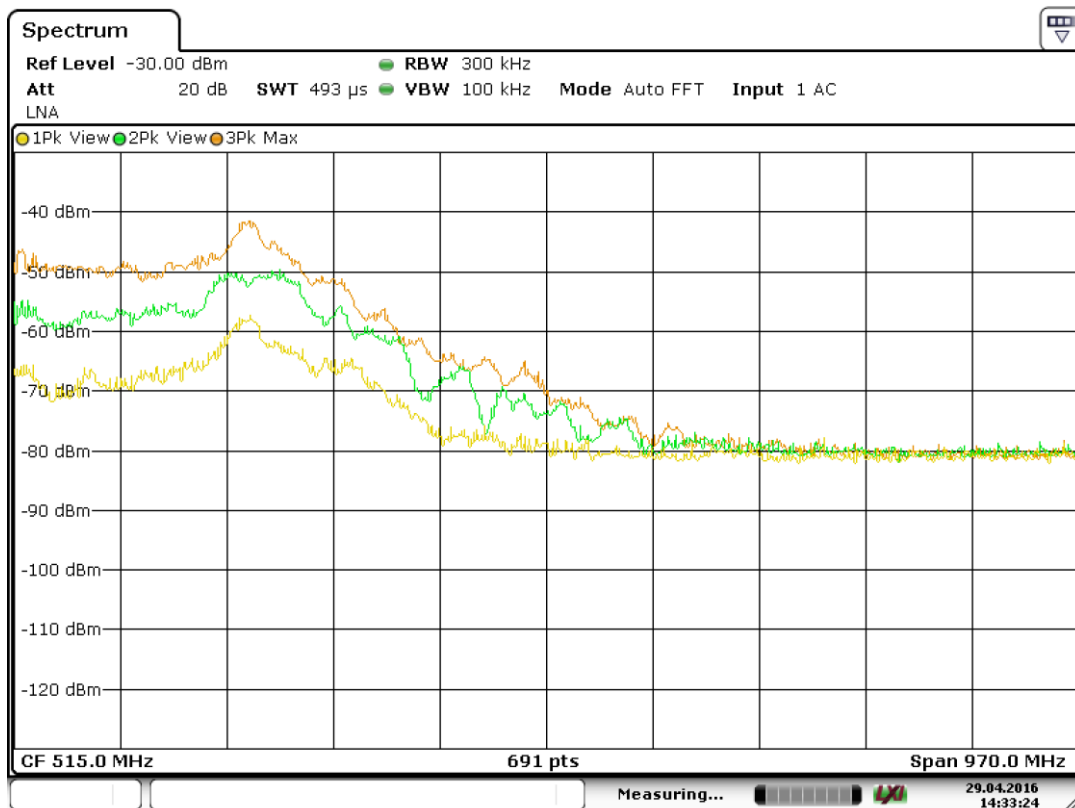


FIGURE 42. TPS62110 NEAR-FIELD EMI RESULTS (YELLOW 0.1 A, GREEN 0.5 A, ORANGE 1.5 A)

TABLE 10. BATTERY MANAGEMENT SYSTEM CHARGE VOLTAGE DROP MEASUREMENT RESULTS

Load current (A)	Unidirectional (mV)						Bidirectional (mV)					
	LTC4226			LTC4228			LTC4226			LTC4228		
	8.4 V	7.4 V	6.6 V	8.4 V	7.4 V	6.6 V	8.4 V	7.4 V	6.6 V	8.4 V	7.4 V	6.6 V
0.1	175	172	171	23.7	23.7	23.7	4.5	4.3	4.5	23.7	23.7	23.7
0.25	206	203	203	23.8	23.8	23.8	11.5	11.5	11.2	23.7	23.8	23.8
0.5	234	232	232	23.8	23.8	23.8	23	23	23.1	23.8	23.9	23.9
0.75	256	253	253	29.4	29.3	29.4	34.7	34.8	34.7	29.4	29.4	29.4
1	267	270	270	39.2	39.2	39.2	46.3	46.3	46.3	39.2	39.2	39.2
1.25	285	285	285	49.1	48.9	49.2	58	58	58	49.2	49.1	49.1
1.45	298	297	297	57.1	57.1	57.1	67.3	67.3	67.2	57.1	57.1	57.1

TABLE 11. BATTERY MANAGEMENT SYSTEM DISCHARGE VOLTAGE DROP MEASUREMENT RESULTS

Load current (A)	Unidirectional (mV)						Bidirectional (mV)					
	LTC4226			LTC4228			LTC4226			LTC4228		
	8.4 V	7.4 V	6.6 V	8.4 V	7.4 V	6.6 V	8.4 V	7.4 V	6.6 V	8.4 V	7.4 V	6.6 V
0.1	177	174	173	28.8	28.6	28.6	4.6	4.6	4.6	28.8	28.8	28.8
0.25	207	204	203	28.8	28.6	28.7	11.5	11.5	11.5	28.8	28.8	28.8
0.5	235	232	230	28.8	28.7	28.7	23.1	23.1	23	28.8	28.8	28.8
0.75	255	253	252	28.8	28.7	28.7	34.8	34.8	34.8	28.8	28.8	28.8
1	272	270	270	28.8	28.7	28.7	46.4	46.4	46.4	28.8	28.8	28.9
2	330	330	328	28.9	28.8	28.8	93.1	93	93	28.9	28.9	28.9
3	380	380	378	41.4	41.5	41.6	140	139	139	41.5	41.3	41.1
4	427	426	426	55.4	55.9	55.8	187	187	186	55.4	55.3	55.1
5	475	470	470	70.1	70.3	70.4	234	234	233	70.2	69.6	69.3
6	0	0	0	85.2	85.1	85.3	277	277	277	85.1	85	84.2

Non-exclusive licence to reproduce thesis and make thesis public

I, Erik Ilbis (date of birth: 21.03.1991), herewith grant the University of Tartu a free permit (non-exclusive licence) to:

1.1. reproduce, for the purpose of preservation and making available to the public, including for addition to the DSpace digital archives until expiry of the term of validity of the copyright, and

1.2. make available to the public via the web environment of the University of Tartu, including via the DSpace digital archives until expiry of the term of validity of the copyright,

System Architecture and Component Evaluation for ESTCube-2 Electrical Power System supervised by Dr. Mihkel Pajusalu and Artur Abels.

2. I am aware of the fact that the author retains these rights.

3. I certify that granting the non-exclusive licence does not infringe the intellectual property rights or rights arising from the Personal Data Protection Act.

Tartu, 20.05.2016